Modelling circular optical microresonators using whispering gallery modes

Ellen Franchimon
0040789
July 30, 2010

Supervisor:
dr. M. Hammer

Committee:
prof. dr. E. van Groesen
dr. M. Hammer
dr. H.J.W.M. Hoekstra

UNIVERSITEIT TWENTE.

Applied Mathematics
Chair AAMP

Abstract

The growth of the Internet during the past years led to an increased demand for capacities in long distance communication. This was partly met by techniques for all optical multiplexing. One of the ways to multiplex optical signals is using a circular optical microresonator. A circular cavity can act as an optical filter by placing it between two straight waveguides. Light is launched into one of these. If the input wavelength matches the cavity a resonance will occur and the power will be transferred to the other waveguide. Otherwise, no resonance occurs and the light will stay in the first waveguide.

This thesis treats ring and disc microresonators within a 2D model. The resonant electomagnetic fields supported by such a free circular cavity are determined in the form of whispering gallery modes. From the Maxwell equations an ansatz for the electric field is derived and from that the resonances are calculated. For this a Matlab program was written which solves for the complex resonance frequency, but needs a good estimate as starting point. The simulation results agree well with the results from [9] and [16].

Once all fields of the cavity and the waveguides are known their interaction has to be determined. For this, a coupled-mode ansatz for the total fields is made, with at first unkown amplitudes. The amplitude functions of the waveguide modes are discretized into finite elements. A weak formulation of the Maxwell equations is used to calculate the amplitudes of all fields. The formalism has been implemented in Matlab. First, only solutions for two straight waveguides were calculated. Coupling occurs if the two waveguides are close enough to each other. The results including a disc or ring cavity match the results from [9]. In all cases the results are as expected.

Contents

Chapter 1

Introduction

Nowadays it is almost impossible to imagine a world without long distance communication. There would be no Internet, no telephone, no radio or television etc. Nevertheless optical based telecommunication is still a young area. The first time a electronic message was sent over a long distance was in 1844, by Samuel Morse. This led to the establishment of telegraphy. Years later, in 1876 Alexander Graham Bell found a way to transmit speach over long distances [20], which resulted in the founding of the first telephone company two years later.

In the years that followed the number of telephone calls grew rapidly, about halfway the twentieth century it became clear that the demand for communication capacity would soon be too large for the current facilities. A new way of transmitting the signal had to be found. Several solutions where suggested, but after a while it turned out that the use of optical fibres was the most feasible [5]. This was, amongst others, made possible by the discovery of the laser in the 1960's.

The first optical fibres were not very suitable for long distance communication, but when their possibilities were recognised a lot of research was done in this area and is still in progress. Nowadays fibres can transmit millions of phone calls simultaneously. However, the demand has grown very rapid as well. Not only for phone calls, but the Internet grows rapidly and more and more people use it to watch video. This ever growing demand asks for growth in the capacity as well. The current fibres have a large capacity, but the modulation and multiplexing is the bottleneck. This is still mainly done by transforming the optical signal into an electrical signal, then modulate or multiplex it and then transform it back to an optical signal [17]. This is not only elaborate, but also relatively slow, since electrical modulation or multiplexing is much slower than optical modulation or multiplexing. Optical modulation and multiplexing could be much faster and there is a lot of research going on to make this possible on large scale. There are several ways to do this. Two important fields of research are photonic crystals and microresonators. Photonic crystals are promising, but at this moment still difficult to fabricate [21]. The technology to fabricate microresonators is better known, so at this moment they are a good candidate.

1.1 Microresonator

One of the options for an optical filter is a microresonator. The coupling to waveguides or other cavities can be either vertically [13], with the cavity above the waveguides, or horizontally, with the waveguides in the plane of the cavity. In this thesis only the simple 2D configuration as shown in figure 1.1 is considered. The coupling between the waveguides and the cavity is horizontal and it
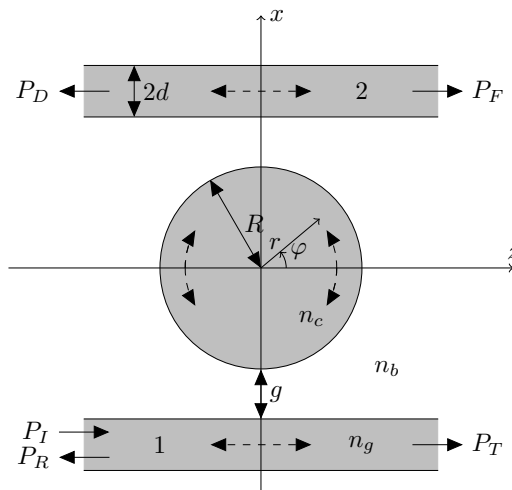

Figure 1.1: A disc microcavity coupled to two straight waveguides.

is assumed that the structure extends infinitely in the third direction. A signal enters through the lower waveguide and will partly couple to the cavity. If the wavelength corresponds to the cavity resonance, the field within the cavity will build up and most of the power will go in there. This implies that almost nothing will go through the lower waveguide. In the top waveguide the situation is reversed. Due to the high power in the cavity part of the light will be coupled into this waveguide. If the wavelength does not match, no resonance will occur. As a result the field does not build up in the cavity and hence no power is coupled to the upper waveguide. These kind of cavities can be used in several ways. The simplest way is simply couple them to two waveguides as described above. They can also be cascaded, this way it is possible to filter out exactly one resonance frequency. Another options is to use them to create a filter array by taking a waveguide in one direction and several waveguides perpendicular to it. Cavities can be placed in the corners and couple different frequencies to different perpendicular waveguides [21].

The aim of this project is to find the resonant frequencies, and hence wavelengths, for such a cavity. This is done by finding the modes of the free cavity (i.e. cavity without adjacent waveguides). Once these resonances are found, the cavity will be coupled to two straight waveguides. For this, a variant of coupled mode theory will be used, together with a finite element discretization for the mode amplitudes of both straight waveguides, based on [8].

1.2 Different approaches

For the calculation of the resonances of a circular cavity two methods are well known, both of them consider the problem in a different way. First there is the bent waveguide approach, figure 1.2 shows how the problem is approached in [10]. In this case a model for the fields of bent waveguide segments that form the cavity is made. The total resonator from figure 1.1 then consists of four parts, two bent-straight waveguide couplers and two bent waveguides. The couplers are linked through the bent waveguides to form the resonator. As is the case with straight waveguides, bent waveguides are analysed with a real frequency. A bent waveguide will always be lossy. These losses are expressed in the wavenumber. For straight waveguides this wavenumber is a real number, but in a bent waveguide the wavenumber will be complex. A disadvantage of this method is that Bessel functions of complex order occur, which are difficult to calculate numerically.
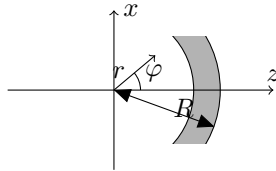
Figure 1.2: A bent waveguide, which is a piece of a circular cavity.

The other approach, a description in terms of whispering gallery modes, looks at the entire cavity as shown in figure 1.3. This method is used in [16] and [18] and will be used in this thesis. The only way to get resonance is if the field after one roundtrip is exactly equal to the original field. This condition is used to establish an expression for the fields. In this case, the solution will have a complex frequency, where the imaginary part accounts for the losses. This is why this approach is sometimes named the complex frequency approach. Finding this complex frequency is complicated, because it is a search for a zero in the complex plane and the respective function changes very gradually along the imaginary axis, but rather rapidly along the real axis.
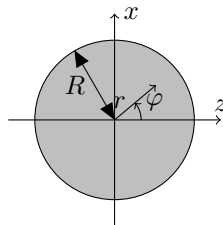
Figure 1.3: The whispering gallery modes are found by considering the cavity as a whole.

Once the resonances of the cavity are found, the coupling between the waveguides and the cavity has to be determined. There are several ways to do this. Mostly a bent-straight waveguide coupler is considered, which is analysed using an approach based on coupled mode theory, see [11] and [18]. However [14] makes use of a pertubation argument and [3] proposes an approach based on Greens function.

The approaches described above are largely analytical. The structure can also be analysed numerically, for instance with an FDTD method (Finite Difference Time Domain), see for instance [12] and [19]. Even in a 2D setting, the calculations are very time consuming. More analytical approaches can reduce this calculation time significantly [14]. These fully numerical methods are often used to verify more analytical methods. For design purposes they take too much time.

In this work a new way of modelling the resonator device is introduced. As mentioned before, the cavity fields will be modelled as whispering gallery modes and the coupling will be estimated by a variant of coupled mode theory, in contrary to approaches used in other publications, where the coupling is determined based on fields of bent waveguides.

1.3   Outline

The remainder of this thesis is organized as follows. The second chapter describes the theory which is needed to find the guided mode of a single-mode waveguide and the whispering gallery modes. This extends from the Maxwell-equations to the actual calculation of such modes. Then, chapter 3 gives some results from the calculations to find the resonances of ring and disc cavities. Those results are compared with results from [16] and [9]. Chapter 4 deals with the theory of the coupling between the fields of the cavity and the waveguides. For this, the mode amplitudes of the waveguides are discretized in the horizontal direction (i.e. along z, see figure 1.1) and then the problem is solved with a finite elements method. Results are discussed in chapter 5. This includes coupling two straight waveguides and coupling a microdisc cavity to two straight waveguides. Finally, chapter 6 gives some conclusions and suggestions for further research.

Chapter 2

Basics

This chapter is the theoretical basis of the thesis. Here the model properties of both straight waveguides and circular cavities will be discussed. It starts in section 2.1 with the Maxwell equations and it is described how they can be used in this specific situation. Section 2.2 shows step by step how the electric field of a straight waveguide can be determined. Section 2.3 does the same for a disc and a ring. This model can easily be extended to circular cavities of more layers.

2.1 The Maxwell equations

The first step in any problem in electromagnetics is to look at the Maxwell equations. In this case the source and charge free version can be used.

The Maxwell equations are then given by

$$\nabla \times \mathbf{E} = -\mu \frac{\partial \mathbf{H}}{\partial t}, \tag{2.1a}$$

$$\nabla \times \mathbf{H} = \varepsilon \frac{\partial \mathbf{E}}{\partial t}, \tag{2.1b}$$

$$\nabla \cdot \mathbf{H} = 0, \tag{2.1c}$$

$$\nabla \cdot \varepsilon \mathbf{E} = 0. \tag{2.1d}$$

Here $\mathbf{E}$ denotes the electric field, $\mathbf{H}$ the magnetic field, ε indicates the permittivity and μ the permeability. In relevant media $\mu \approx \mu_0$ holds at optical frequencies, where μ_0 is the permeability of vacuum.

Furthermore, it is assumed that the structure and the fields are constant in the y-direction. Since all fields will be time harmonic the time dependence can be described by $e^{-i\omega t}$, with ω the frequency, which in general is a complex number.

The second step is to reduce these equations to a more convenient form. This

can be done by filling in the time-derivatives and writing equations (2.1a) and (2.1b) in components. In Cartesian coordinates this looks like

$$\begin{bmatrix} \frac{\partial E_z}{\partial y} - \frac{\partial E_y}{\partial z} \\ \frac{\partial E_x}{\partial z} - \frac{\partial E_z}{\partial x} \\ \frac{\partial E_y}{\partial x} - \frac{\partial E_x}{\partial y} \end{bmatrix} = i\omega\mu_0 \begin{bmatrix} H_x \\ H_y \\ H_z \end{bmatrix} \tag{2.2}$$

and

$$\begin{bmatrix} \frac{\partial H_z}{\partial y} - \frac{\partial H_y}{\partial z} \\ \frac{\partial H_x}{\partial z} - \frac{\partial H_z}{\partial x} \\ \frac{\partial H_y}{\partial x} - \frac{\partial H_x}{\partial y} \end{bmatrix} = -i\omega\varepsilon \begin{bmatrix} E_x \\ E_y \\ E_z \end{bmatrix}. \tag{2.3}$$

The problem treated here is constant along y and the solutions which are relevant are invariant in the y-direction. Hence all y-derivatives will vanish. Now these equations split up into two independent sets. The first involves E_y, H_x and H_z and the second E_x, E_z and H_y. These are associated with TE and TM polarization respectively. This thesis only deals with TE polarization. The relevant equations are

$$H_x = \frac{1}{-i\omega\mu_0} \frac{\partial E_y}{\partial z}, \tag{2.4a}$$

$$H_z = \frac{1}{i\omega\mu_0} \frac{\partial E_y}{\partial x}, \tag{2.4b}$$

$$-i\omega\varepsilon E_y = \frac{\partial H_x}{\partial z} - \frac{\partial H_z}{\partial x} \tag{2.4c}$$

$$= \frac{-1}{i\omega\mu_0} \left(\frac{\partial^2 E_y}{\partial z^2} + \frac{\partial^2 E_y}{\partial x^2} \right). \tag{2.4d}$$

Rewriting the last equation gives

$$0 = \left[\frac{\partial^2}{\partial x^2} + \frac{\partial^2}{\partial z^2} + \omega^2 \mu_0 \varepsilon \right] E_y$$

$$= \left[\nabla^2 + \omega^2 \mu_0 \epsilon \right] E_y. \tag{2.5}$$

Now write $\varepsilon = \varepsilon_0 \varepsilon_r$, with ε_0 the vacuum permittivity, and $\varepsilon_r = n^2$, with n the refractive index of the material, to express this in terms of the speed of light $c^2 = \frac{1}{\mu_0 \varepsilon_0}$. Then equation (2.5) becomes

$$\left[\nabla^2 + \frac{\omega^2 n^2}{c^2} \right] E_y = 0. \tag{2.6}$$

In the structures treated in this thesis there will be jumps in the refractive index profile. At such an interface some continuity conditions have to be satisfied. The first condition is that the y-component of the electric field must be continuous across the interface. The second condition states that all components of the magnetic field should also be continuous.

2.2 The fundamental mode of a straight waveguide

In this section a solution for the electric field of guided waves in a straight waveguide, as shown in figure 2.1, is determined, with the restriction that the refractive indices below and above the waveguide are equal. In this thesis only a
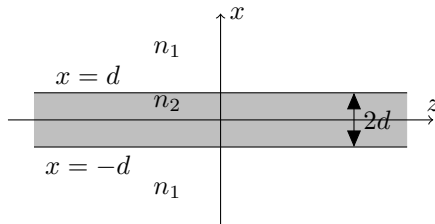

Figure 2.1: A straight waveguide of thickness $2d$, with refractive index n_1 in the cladding and n_2 in the core.

solution corresponding to the fundamental mode will be considered. The field is assumed to propagate in the z-direction with propagation constant β, described by a z-dependence of $e^{i\beta z}$, for a given real frequency ω. Substituting this into equation (2.6) and replacing $\frac{\omega}{c}$ by the wavenumber k leads to

$$\left[\frac{\partial^2}{\partial x^2} - \beta^2 + k^2 n^2 \right] E_y(x) = 0. \qquad (2.7)$$

Of course, the total field looks like $E(x, z, t) = E_y(x)e^{i(\beta z - \omega t)}$. Note that for notational convenience the symbol E_y is re-used here for the x-dependent mode profile.

Recall that at each interface, both the electric field and the component of the magnetic field which is tangential to the interface should be continuous. Furthermore, to form a guided mode the field should be decaying in the areas outside the waveguide and be confined to the waveguide. Since only the fundamental mode is required, the search is for a solution of equation (2.7) which behaves like a cosine in the waveguide region [6, 15].

Thanks to the symmetry the mode profile is a solution of equation (2.7) in the form

$$E_y(x) = \begin{cases} Be^{\alpha x} & \text{for } x \leq -d, \\ A\cos(\gamma x) & \text{for } -d < x < d, \\ Be^{-\alpha x} & \text{for } x \geq d, \end{cases}$$

with $\alpha = \sqrt{\beta^2 - k^2 n_1^2}$ and $\gamma = \sqrt{k^2 n_2^2 - \beta^2}$.

As mentioned before the E_y-field should be continuous at $x = \pm d$. The same holds for the z-component of the magnetic field, hence equation (2.4b) implies that the x-derivative of E_y should also be continuous at $x = d$ and $x = -d$. It

is easy to see that the equations at $x = d$ are exactly equal to those at $x = -d$. This is due to the symmetry of the structure. In matrix form this can be written as

$$\left[\begin{array}{cc} \cos(\gamma d) & -e^{-\alpha d} \\ -\gamma \sin(\gamma d) & \alpha e^{-\alpha d} \end{array} \right] \left[\begin{array}{c} A \\ B \end{array} \right] = 0.$$

Such a system of equations has a nontrivial solution if and only if

$$\det \left[\begin{array}{cc} \cos(\gamma d) & -e^{-\alpha d} \\ -\gamma \sin(\gamma d) & \alpha e^{-\alpha d} \end{array} \right] = 0.$$

Remember that β, which is hidden in α and γ, is the primary unknown. Since it is not possible to solve this equation analytically for β [2], a numerical solution has to be found.

As soon as the value of β is known, the ratio between the constants A and B can be calculated and the electric field can be determined everywhere up to an arbitrary complex constant. In figure 2.2 an example of a snapshot of the electric field of a waveguide is shown. Note that here only the real part of the total field, including the time dependence, is shown at an arbitrary time, this is the physical part. This will be the case in all of the figures in this thesis. For positive β, in time this field moves in the positive z-direction. The field will oscillate, but not decay in time.
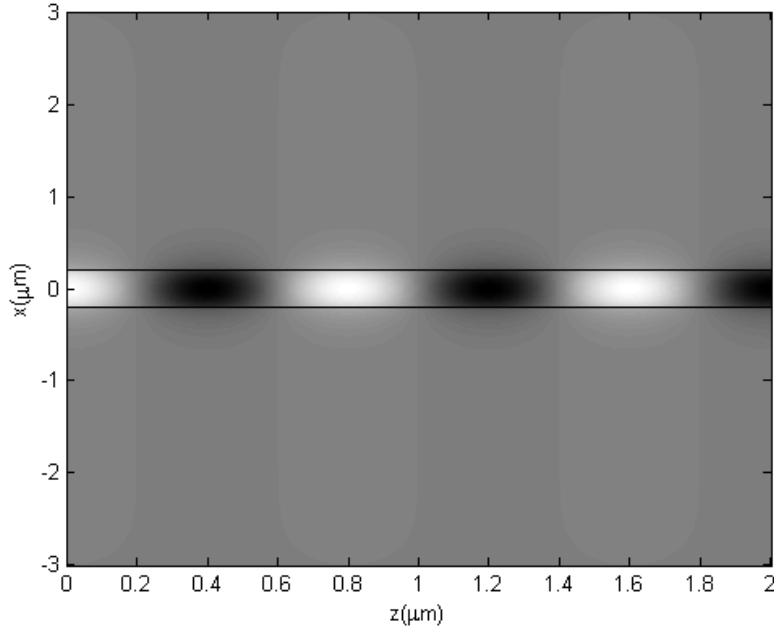

Figure 2.2: The modal electric field of a waveguide with $d = 0.2\mu m$, $n_1 = 1.0$, $n_2 = 1.5$ and $\lambda = 1.05\mu m$.

2.3 Whispering gallery modes

This section explains how the electric field of a disc or ring cavity as shown in figure 2.3 can be calculated. This model can also be used for structures with more layers. The layers are numbered in increasing order from the inner layer to the outer layer. Thus the layer containing the origin will be denoted as layer 1, the layer surrounding it as 2, etc.
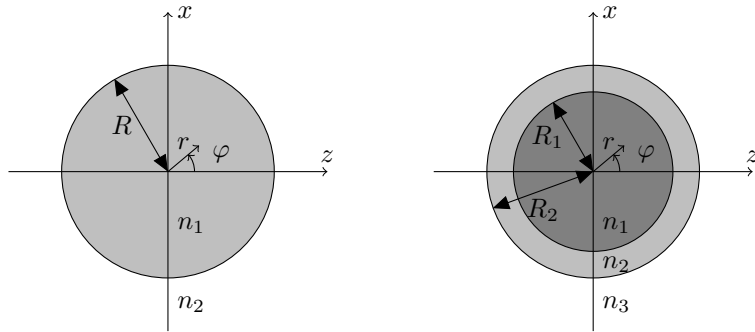

Figure 2.3: Left: A disc with radius R. Right: A ring with radii R_1 and R_2 The refractive indices are numbered in increasing order from the centre.

In this thesis the search is for a resonant solution, where the field should oscillate harmonically in time. This oscillating behaviour is described by a time dependence of $e^{-i\omega t}$, in this case ω can be a complex number. Since the field of such a cavity will always be lossy, the physically relevant solution should also decay in time, hence the imaginary part of frequency ω should be negative. That way the real part of $-i\omega t$ will be negative and the desired decay in time is obtained. The real part of ω should be close to a given target frequency. Sometimes the target wavelength λ is given, the relation between λ and the real part of ω is then $Re(\omega) = 2\pi c/\lambda$.

Because of the circular symmetry in the structure it is an obvious choice to use cylindrical coordinates (r, φ). To get the desired resonance the fields should be exactly equal to the original fields after making one roundtrip. This results in an angular dependence $e^{im\varphi}$ of the electric field, where m is an integer. Hence the electric field has the form $E(r, \varphi, t) = E_y(r)e^{i(m\varphi - \omega t)}$. Note that here the symbol E_y has been re-used again.

Substitute all this into equation (2.6) to obtain the radial equation

$$\left[\frac{\partial^2}{\partial r^2} + \frac{1}{r}\frac{\partial}{\partial r} + \frac{\omega^2 n^2}{c^2} - \frac{m^2}{r^2} \right] E_y(r) = 0.$$

Multiplication by r^2 gives the Bessel equation

$$\left[r^2\frac{\partial^2}{\partial r^2} + r\frac{\partial}{\partial r} + r^2\frac{\omega^2 n^2}{c^2} - m^2 \right] E_y(r) = 0. \tag{2.8}$$

9

Solutions of this equation are the Bessel functions J and Y. Based on the boundary conditions, a suitable combination of the fundamental solutions J and Y has to be chosen for each region. These conditions are:

- At the origin the fields should be finite.

- At each interface the continuity conditions mentioned in section 2.1 should hold. This means that both the electric field and the component of the magnetic field which is tangential to the interface should be continuous. Using equation 2.1a, the second condition implies that the r-derivative of E_y is continuous.

- In the outer layer the waves should be outgoing.

In equation (2.8) m only appears quadratically, hence the solutions for $\pm m$ are identical. In this thesis the counter clockwise rotation is chosen with m positive. In the layer which includes the origin the only possible solution is the Bessel function of the first kind, since this is the only Bessel function which is finite in the origin. So in this layer the field will be described by

$$E_y(r) = a_1 J_m(\frac{\omega}{c} n_1 r).\tag{2.9}$$

Here n_1 is the refractive index of layer 1. The constant a_1 is unknown for the moment. In all the layers (possibly none) which are present between the inner and the outer layer no further conditions are given, hence in this region a combination of the Bessel functions of the first and second kind should be used. The electric field will then be

$$E_y(r) = a_{2k-2} J_m(\frac{\omega}{c} n_k r) + a_{2k-1} Y_m(\frac{\omega}{c} n_k r).\tag{2.10}$$

Constants a_{2k-2} and a_{2k-1} are currently undefined, they will be determined later on. Here k denotes the number of the layer, counting starts with one at the inner layer.

In the outer region the requirement is that the waves should be outgoing. The only solution which has this property for the time dependence considered here is the Hankel function of the first kind. Hence in this region the electric field is described by

$$E_y(r) = a_{2K-2} H_m^{(1)}(\frac{\omega}{c} n_K r),\tag{2.11}$$

where $k = 1, ..., K$ and K is the number of layers.

As mentioned before at the boundaries both the electric and the magnetic field should be continuous. From equation (2.1a) it is clear that the magnetic field is a constant times the r-derivative of the electric field. These conditions are needed to find all constants $a_1...a_{2K-2}$ from equations (2.9)-(2.11). All these conditions can be written in the form $Aa = 0$, where a is the vector consisting of all the constants a_j and A is a matrix. This matrix has $2(K-1)$ rows: two rows for each interface, the first represents continuity conditions for the electric field and the second continuity conditions for the magnetic field. On each row

only the entries corresponding to the layers next to the interface are nonzero. For two layers, thus the situation of the disc, this results in

$$
A = \begin{bmatrix} J_m(\frac{\omega}{c}n_1R_1) & -H_m^{(1)}(\frac{\omega}{c}n_2R_1) \\ \frac{\omega}{c}n_1 J'_m(\frac{\omega}{c}n_1R_1) & -\frac{\omega}{c}n_2 H_m^{(1)\prime}(\frac{\omega}{c}n_2R_1) \end{bmatrix}.
$$

Here the prime denotes a derivative with respect to the argument. See appendix B for more detail on these derivatives. For three layers, the ring, it looks like

$$
A = \begin{bmatrix} J_m(\frac{\omega}{c}n_1R_1) & -J_m(\frac{\omega}{c}n_2R_1) & -Y_m(\frac{\omega}{c}n_2R_1) & 0 \\ \frac{\omega}{c}n_1 J'_m(\frac{\omega}{c}n_1R_1) & -\frac{\omega}{c}n_2 J'_m(\frac{\omega}{c}n_2R_1) & -\frac{\omega}{c}n_2 Y'_m(\frac{\omega}{c}n_2R_1) & 0 \\ 0 & J_m(\frac{\omega}{c}n_2R_2) & Y_m(\frac{\omega}{c}n_2R_2) & -H_m^{(1)}(\frac{\omega}{c}n_3R_2) \\ 0 & \frac{\omega}{c}n_2 J'_m(\frac{\omega}{c}n_2R_2) & \frac{\omega}{c}n_2 Y'_m(\frac{\omega}{c}n_2R_2) & -\frac{\omega}{c}n_3 H_m^{(1)\prime}(\frac{\omega}{c}n_3R_2) \end{bmatrix}.
$$

This can easily be extended to more layers, just by adding extra rows with the proper input. The matrix will always be square, because each additional layer adds two rows, one for the electric and one for the magnetic field, and two columns, since the extra layer will be a layer in the region between the inner and the outer layer and thus has a component for the Bessel function of the first and the second kind. The system $Aa = 0$ only has a nontrivial solution if the determinant of A is zero. Using this requirement ω can be determined for a given m.

This is not as simple as it seems. Since ω is a complex number, the search is in fact for a combination of two real quantities. Furthermore, there are several solutions which in some cases are very close to each other. This means it is necessary to make a very good initial guess. In the configurations considered in this report this is done by making a plot of $|\det(A)|$ and then manually look where the required minimum is approximately located. This value is then inserted in Matlab's numerical iterative solver fsolve and if the guess is good enough the right value for ω will be found.

Once ω is known the vector a can be calculated up to a constant and hence the total electric field can be determined. Figure 2.4 shows an example of a snapshot of the electric field of a disc.

As soon as the $E_y(r)$ is known, the total field is determined by multiplying it with $e^{i(m\varphi - \omega t)}$. As mentioned before, the general behaviour will be that the field starts to rotate in a counter clockwise direction. Since the whispering gallery modes are lossy by definition, the light will travel in an outward direction and the fields in the cavity will decay in time.
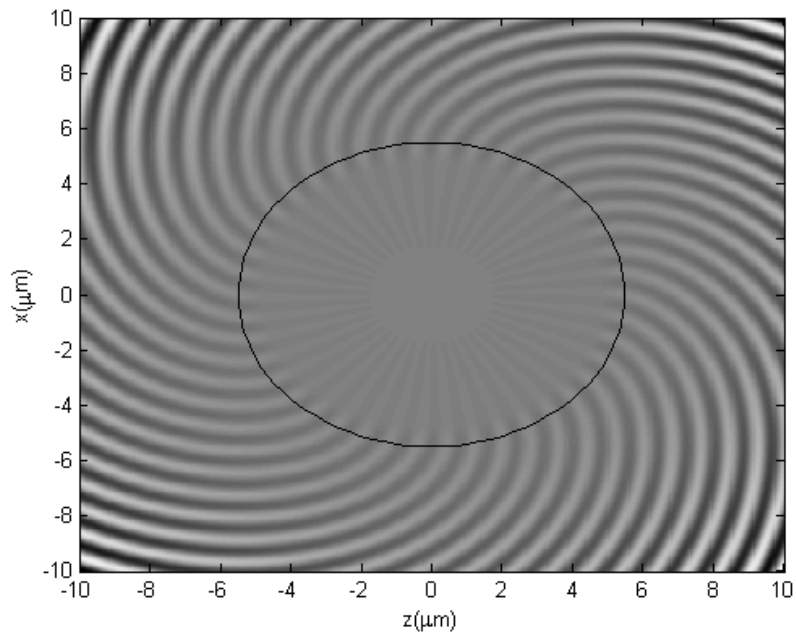
Figure 2.4: The electric field of a disc with $n_1 = 1.7$, $n_2 = 1.6$, $r = 5.5\mu m$ and $\lambda \approx 1.3\mu m$.

Chapter 3

Numerical results

This chapter gives some numerical results obtained with the Matlab code written to solve for the resonant fields of discs and rings as explained in chapter 2. To check whether this model and the accompanying code are correct, the results are compared to reference results from the literature. This will also help to get some intuition for the behaviour of such a cavity. Section 3.1 compares the results mentioned in [16] to the results of this code. Section 3.2 looks at higher order modes and compares these with the results from [9].

3.1 Ring and disc cavities

First the results from this program are compared to the results for the ring and disc cavities from [16]. This article also makes use of whispering gallery modes, so the results should correspond. All values for parameters are chosen exactly equal to those in [16], however it is important to apply the proper definition of the radius, since this is different from the definition used in this thesis. The radius R_c given in that article is the radius of the centre of the ring, where the ring has a thickness of $1\mu m$. Using the notation of figure 2.3 this means that $R_1 = R_c - 0.5\mu m$ and $R_2 = R_c + 0.5\mu m$. For comparison reasons the radius R of the disc is equal to R_2.

The refractive index of the disc or ring is $n = 1.7$ and in the surrounding and the interior of the ring $n = 1.6$. The resonances should be around the wavelength $\lambda = 1.3\mu m$, which results in a real frequency of 1.45PHz. The tested structures have radii of curvature between $R_c = 5\mu m$ and $R_c = 200\mu m$. The value of m is chosen equal to the value given in [16].

In table 3.1 the results for the disc are shown. The results agree well.

$R_c(\mu m)$	m	Frequency from [16](PHz)		Calculated frequency(PHz)	
		$Re(\omega)$	$Im(\omega)$	$Re(\omega)$	$Im(\omega)$
5	42	1.4591	-5.428×10^{-2}	1.4560	-5.397×10^{-2}
10	82	1.4550	-2.016×10^{-2}	1.4544	-2.077×10^{-2}
20	162	1.4501	-4.662×10^{-3}	1.4497	-4.679×10^{-3}
30	243	1.4526	-1.136×10^{-3}	1.4520	-1.315×10^{-3}
40	323	1.4482	-2.580×10^{-4}	1.4480	-2.909×10^{-4}
50	404	1.4483	-5.102×10^{-5}	1.4480	-5.834×10^{-5}
60	485	1.4479	-9.161×10^{-6}	1.4480	-1.198×10^{-5}
80	648	1.4489	-2.407×10^{-7}	1.4498	-4.701×10^{-7}
100	811	1.4491	-5.447×10^{-9}	1.4501	-1.355×10^{-8}
200	1612	1.4497	-1.690×10^{-13}	1.4500	-5.011×10^{-13}

Table 3.1: Disc with varying radius. Whispering gallery modes with eigenfrequencies around 1.45 PHz.

$R_c(\mu m)$	m	Frequency from [16](PHz)		Calculated frequency(PHz)	
		$Re(\omega)$	$Im(\omega)$	$Re(\omega)$	$Im(\omega)$
5	42	1.4590	-5.428×10^{-2}	1.4559	-5.319×10^{-2}
10	82	1.4554	-2.113×10^{-2}	1.4544	-2.011×10^{-2}
20	162	1.4526	-5.748×10^{-3}	1.4508	-5.563×10^{-3}
30	242	1.4515	-2.013×10^{-3}	1.4520	-2.218×10^{-3}
40	322	1.4509	-7.507×10^{-4}	1.4510	-8.326×10^{-4}
50	402	1.4504	-2.819×10^{-4}	1.4500	-3.044×10^{-4}
60	482	1.4499	-1.044×10^{-4}	1.4500	-1.228×10^{-4}
80	642	1.4491	-1.368×10^{-5}	1.4490	-1.631×10^{-5}
100	813	1.4504	-1.685×10^{-6}	1.4500	-2.002×10^{-6}
200	1605	1.4499	-4.343×10^{-11}	1.4500	-7.707×10^{-11}

Table 3.2: Ring with varying radius. Whispering gallery modes with eigenfrequencies around 1.45 PHz.

Table 3.2 shows the results for the ring. Again the results agree very well. From the smaller absolute value of the imaginary part of ω, it can be seen that the light is a little bit better confined in the disc than in the corresponding ring. The reason for this is the higher refractive index in the centre. Figure 3.3 shows the electric field in both the disc and the ring with $R_c = 10\mu m$, the values for m and ω can be found in table 3.1 and 3.2.

An extra indication for the correctness of the code is the continuity of the electric field. Figure 3.1 shows that both the real and the imaginary part of the electric field of the disc are continuous on the interface. Figure 3.2 shows that this is also the case for the ring. These figures just serve as an example, this continuity holds in all other cases as well. In principle also the continuity of the derivative, or of the magnetic field components, would have to be checked.
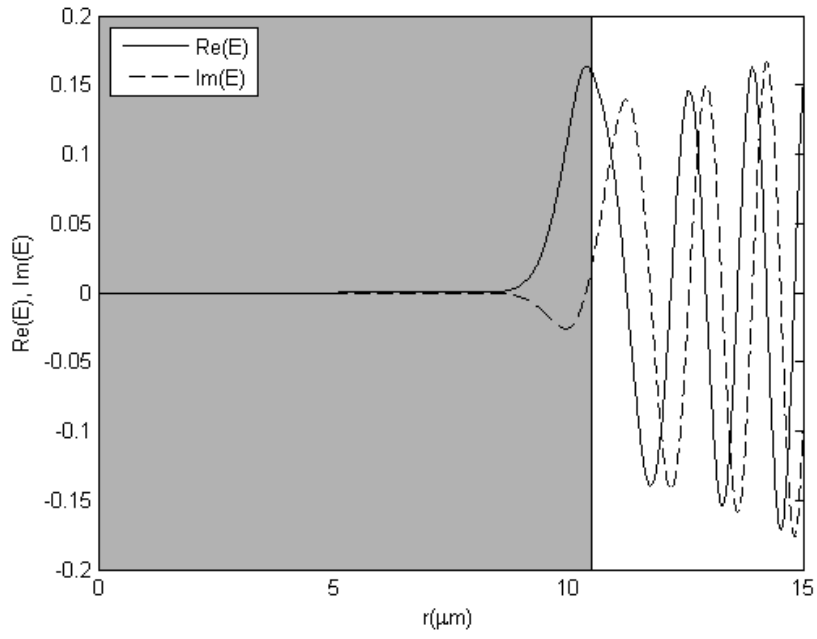
Figure 3.1: The real and imaginary part of the electric field of a whispering gallery mode supported by a disc with radius of curvature $R_c = 10\mu m$, all other parameters are as in table 3.1.
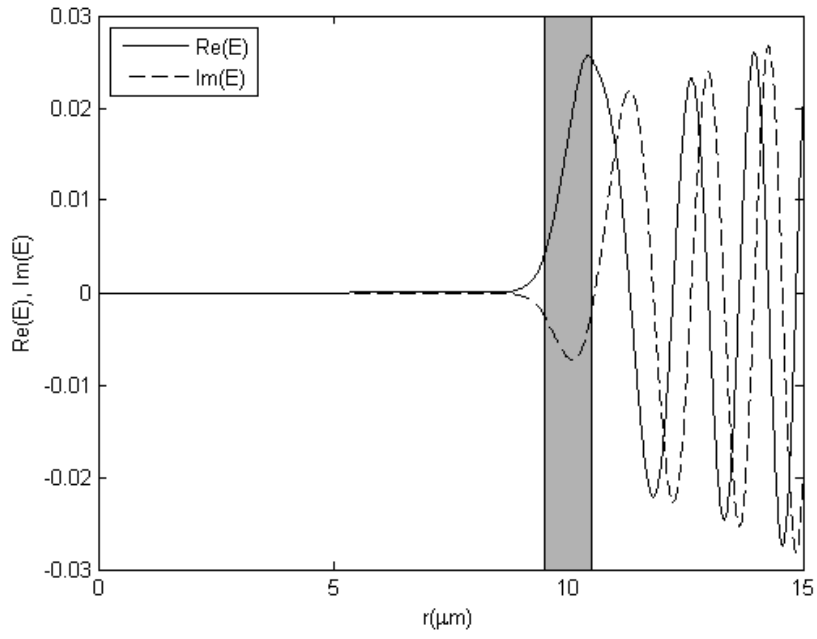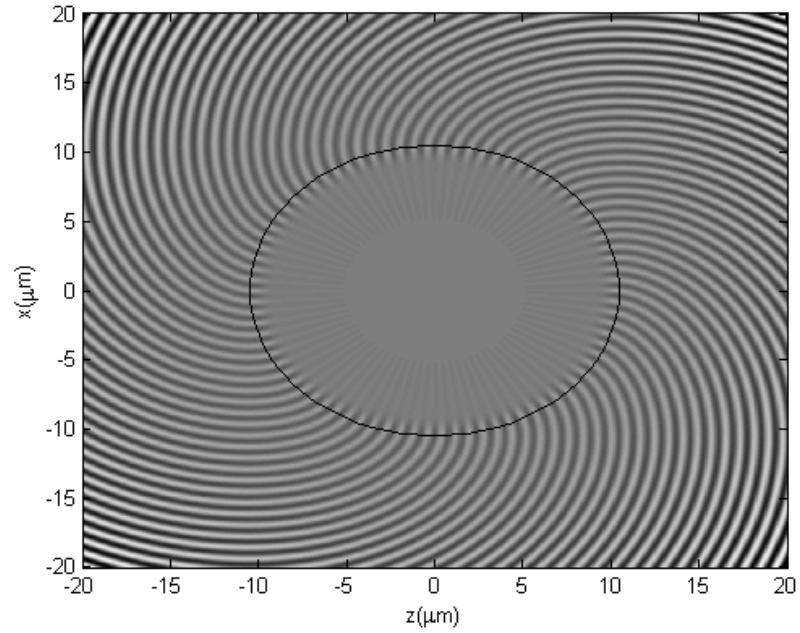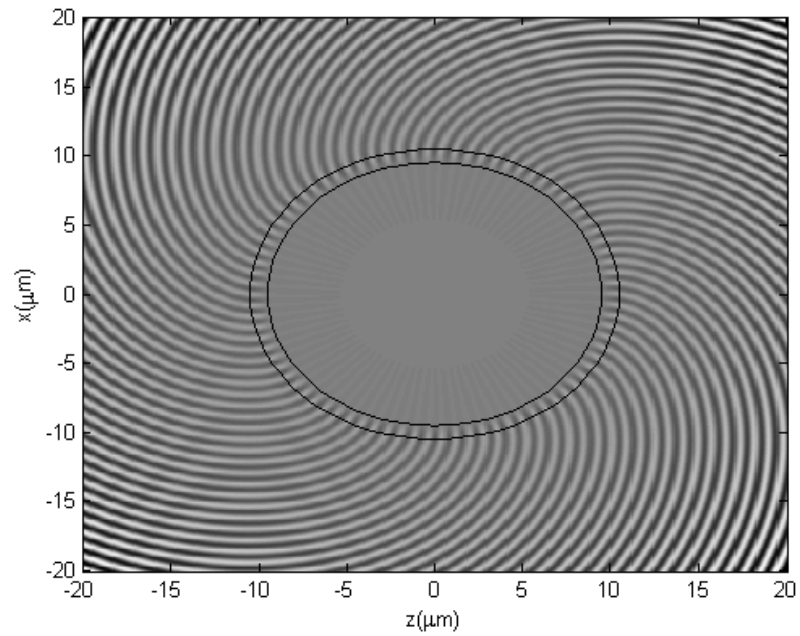
Figure 3.2: The real and imaginary part of the electric field of a whispering gallery mode supported by a ring with radius of curvature $R_c = 10\mu m$, all other parameters are as in table 3.2.

(a)

(b)

Figure 3.3: The electric field of (a) a disc, $\lambda = 1.2951\mu m$, and (b) a ring, $\lambda = 1.2946\mu m$, with $R = 10\mu m$, $m = 82$.

| mode | m | Calculated frequency(Phz) | | Calculated $\frac{mc}{R\omega}$ | $\frac{mc}{R\omega}$ from [9] |
		$Re(\omega)$	$Im(\omega)$		
TE_0	33	1.887	-1.481×10^{-5}	$1.3107 + i1.029 \times 10^{-5}$	$1.3106 - i1.1294 \times 10^{-5}$
TE_1	29	1.910	-2.381×10^{-3}	$1.1380 + i1.419 \times 10^{-3}$	$1.1348 - i1.8862 \times 10^{-3}$
TE_2	25	1.890	-1.616×10^{-2}	$0.9913 + i8.476 \times 10^{-3}$	$0.9902 - i1.1676 \times 10^{-2}$
TE_3	22	1.912	-2.892×10^{-2}	$0.8622 + i1.304 \times 10^{-2}$	$0.8558 - i1.8832 \times 10^{-2}$

Table 3.3: Modes with different radial orders.

## 3.2 Higher order modes in a disc

To check whether the code also works for higher order modes, the structure on page 44 of [9] was tested. This is a disc with a radius of $R = 4.0\mu m$, the refractive indices are $n_1 = 1.5$ and $n_2 = 1.0$. The desired wavelength is $\lambda = 1.0\mu m$, which results in a real frequency of 1.8834PHz. Table 3.3 shows the results and gives the values from [9] as reference. The latter ones are calculated using a bend mode approach, this implies that m is a complex number and ω is real. The results should be comparable, even though the way to obtain them is different, because the physical situation is the same. It turns out that comparing $\frac{mc}{R\omega}$ gives good results. An explanation for this comparison can be found in appendix A.

The modes are indicated with TE because of the polarization. The numbers of the modes indicate the number of zero crossings within the cavity in the radial direction.

The results fit quite well, the only big difference is the sign of the imaginary part of $\frac{mc}{R\omega}$. This difference is due to the use of $e^{i\omega t}$ for the time dependency in [9], where this thesis assumes the time dependence to be $e^{-i\omega t}$. The real part of ω is in both cases positive, because the propagation direction is reversed. However, the sign of the imaginary part of ω is determined by the fact that the real part of the time dependence should describe decaying fields. Hence, in [9] the imaginary part of ω should be positive, where in this thesis it has to be negative. Figure 3.4 shows the electric field of all four described modes.
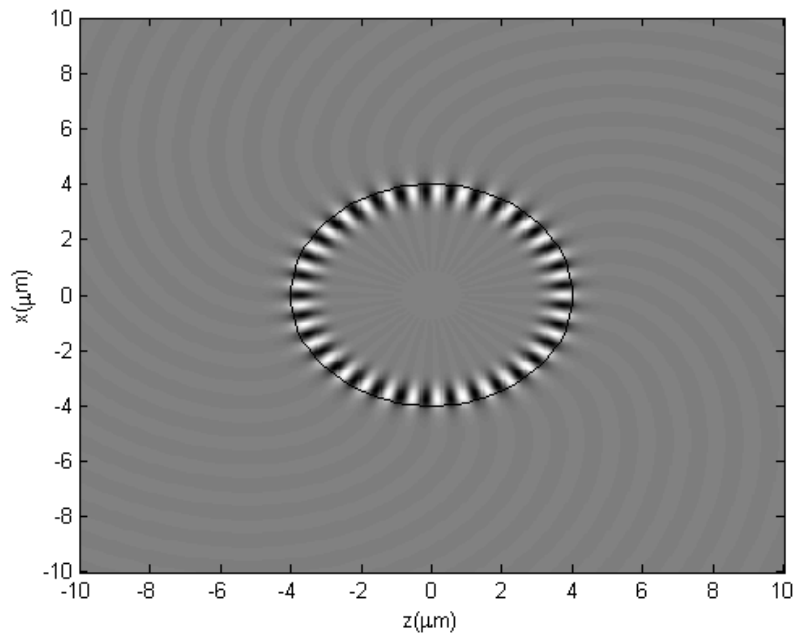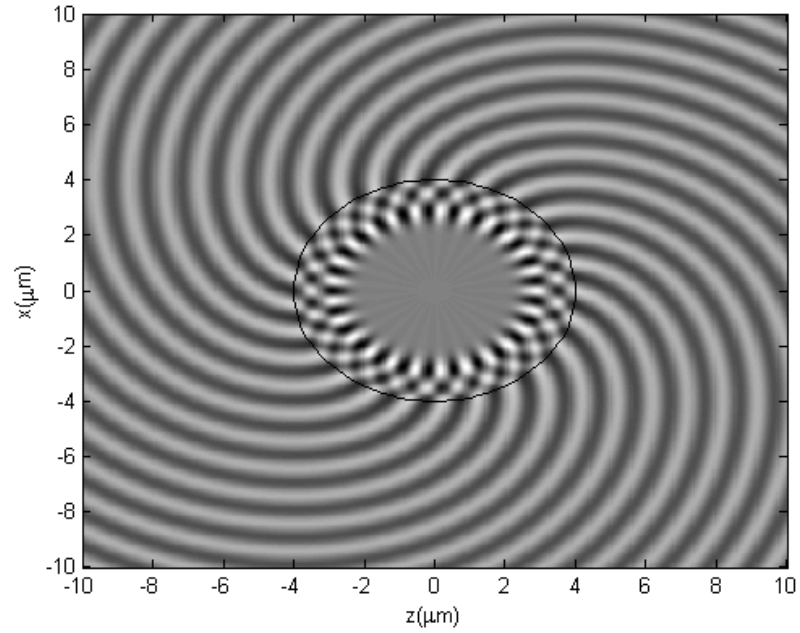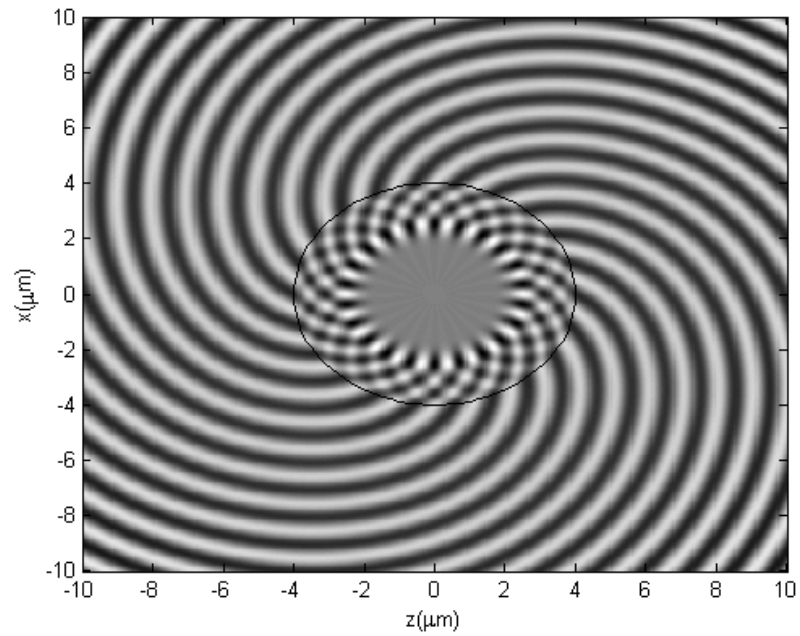
(a) TE_0
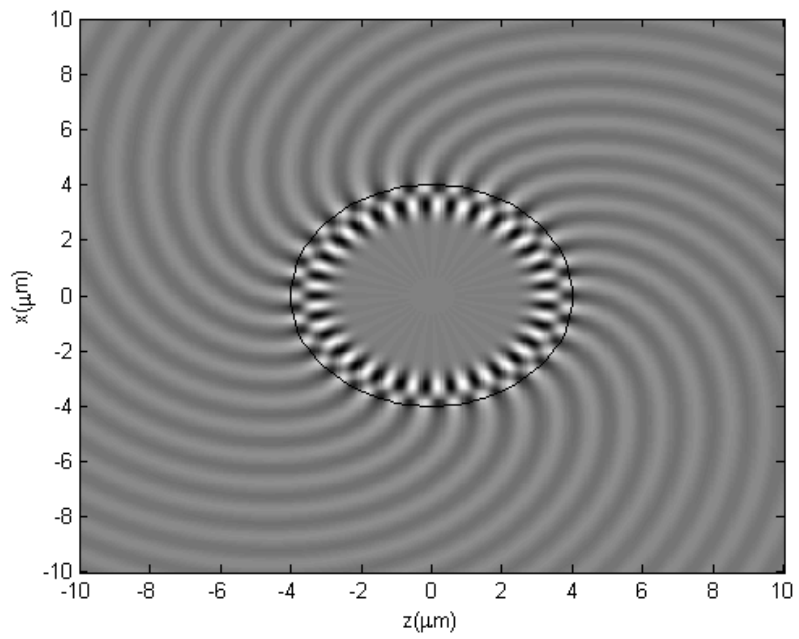
(b) TE_1

Figure 3.4

(c) TE_2

(d) TE_3

Figure 3.4: The electric field of the different modes from table 3.3. The colorscale is chosen individually for each figure, so the levels are not comparable.

Chapter 4

Coupling the waveguides and the cavity

This chapter explains how the waveguides and cavity from chapter 2 can be coupled to form the resonator device shown in figure 4.1. Both parallel waveguides have the same properties like thickness $2d$ and refractive index n_g and are located at a distance g below and above the cavity. The device is excited in the lower waveguide 1 from the left. A part P_T of the incoming power P_I is transmitted to the right outlet of waveguide 1, another part P_D will be transmitted to the left outlet of the upper wavguide 2. A small part P_R of the incoming power will be reflected to the left outlet of waveguide 1 and a part P_F will be transmitted to the right outlet of waveguide 2. The cavity itself has radius R and refractive index n_c. The background index is n_b. Section 4.1 explains how the fields of the waveguides and the cavity are combined into an ansatz for the field of the full device which contains unknowns. A variant of coupled mode theory (CMT) then allows to determine these with a finite elements discretization in the z-direction, as is explained by section 4.2. This approach is based on [8].

4.1   Coupled mode theory

From chapter 2 the electric and magnetic fields of the waveguides and cavity are known. In this analysis only the fundamental mode of each waveguide is taken into account, just as in section 2.2. For the cavity several modes will be used, but strongly radiating modes will be neglected. The fields of the waveguides are of the form

$$\psi_n^\pm(x,z) = \left[\begin{array}{c} \tilde{\mathbf{E}} \\ \tilde{\mathbf{H}} \end{array} \right]_n^\pm (x) e^{\pm i\beta z} \text{ for } n = 1, 2.$$

Here the plus sign indicates a mode propagating to the right and the minus a mode propagating to the left. The subscript n denotes which waveguide the field
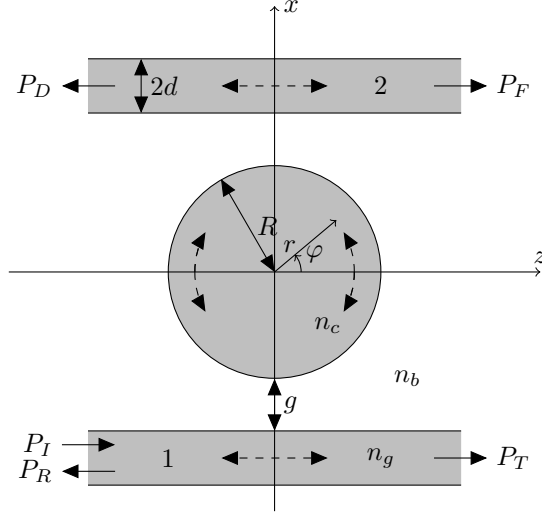
Figure 4.1: The microdisc resonator as investigated in this chapter. The dashed arrows indicate the direction of propagation. The distance between the cavity and the waveguide is indicated with g

corresponds to. $\tilde{\mathbf{E}}$ is the electric part of the mode profile and $\tilde{\mathbf{H}}$ the magnetic part of the mode profile. For the cavity a similar notation is used, namely

$$\psi_3^M(x,z) = \left[\begin{array}{c} \tilde{\mathbf{E}} \\ \tilde{\mathbf{H}} \end{array} \right]_M (x,z).$$

The index M indicates the mode of the cavity. This can be either a counter clockwise propagating mode with a positive angular wavenumber m or a clockwise propagating mode with a negative angular wavenumber.

Now the total field can be expressed as a sum of the former expressions

$$\left[\begin{array}{c} \mathbf{E} \\ \mathbf{H} \end{array} \right] (x,z) = f_1(z)\psi_1^+(x,z) + b_1(z)\psi_1^-(x,z) + f_2(z)\psi_2^+(x,z)$$
$$+ b_2(z)\psi_2^-(x,z) + \sum_M \gamma_M \psi_3^M(x,z). \qquad (4.1)$$

This approximation comes from coupled mode theory. It assumes that the original fields of a component of the structure (i.e. a waveguide or cavity) are not much disturbed by the presence of the other components. Except for the functions f_1, b_1, f_2, b_2 and the coefficients γ_M everything on the right side of equation (4.1) is known.

4.2   Finite elements

The aim is now to determine the unknown amplitudes in equation (4.1). For this finite elements will be used in the z-direction. The quantities f_1, b_1, f_2 and b_2

are functions of z, hence they will be discretized. The horizontal computational window $[z_0, z_N]$ is divided in N pieces of length $\Delta z = (z_N - z_0)/N$. Nodal points are placed at $z_j = z_0 + j\Delta z$, with $j = 0, .., N$. For each node the piecewise linear function $\alpha_j(z)$ is given by

$$\alpha_j(z) = \begin{cases} (z - z_{j-1})/\Delta z & \text{, if } z_{j-1} \leq z < z_j, \\ (z_{j+1} - z)/\Delta z & \text{, if } z_j \leq z < z_{j+1}, \\ 0 & \text{, elsewhere,} \end{cases}$$

with the exception that $\alpha_0 = 1$ for $z < z_0$ and $\alpha_N = 1$ for $z > z_n$.

Using these functions a first order discretization of $f_1(z)$ into linear finite elements is

$$f_1(z) = \sum_j f_j^1 \alpha_j(z).$$

The other amplitudes are discretized in the same way.

The next step is to collect all amplitudes f_j^1, b_j^1, f_j^2 and b_j^2, together with the unknowns γ_M in a big set $\{a_k\}$, or a vector $\mathbf{a}$. The total field from equation (4.1) now looks like

$$\begin{bmatrix} \mathbf{E} \\ \mathbf{H} \end{bmatrix}(x, z) = \sum_k a_k \begin{bmatrix} \mathbf{E}_k \\ \mathbf{H}_k \end{bmatrix}(x, z). \tag{4.2}$$

$\mathbf{E}_k$ and $\mathbf{H}_k$ are an assembly of $\alpha_j(z)\psi_n^{\pm}(x, z)$ and $\psi_3^M(x, z)$. Next the Maxwell equations in the frequency domain are considered in the form

$$\nabla \times \mathbf{E} - i\omega\mu_0\mathbf{H} = 0 \tag{4.3a}$$

$$-\nabla \times \mathbf{H} - i\omega\varepsilon\mathbf{E} = 0. \tag{4.3b}$$

A weak formulation can be obtained by multiplying equation (4.3a) with the complex conjugate (*) of a trial field $\mathbf{H}'$ and equation (4.3b) with the complex conjugate of trial field $\mathbf{E}'$, then add them and integrate the whole thing. The resulting equation is

$$\int\int \left\{ (\mathbf{H}')^* \cdot (\nabla \times \mathbf{E}) - (\mathbf{E}')^* \cdot (\nabla \times \mathbf{H}) - i\omega\varepsilon(\mathbf{E}')^* \cdot \mathbf{E} \right.$$
$$\left. -i\omega\mu_0(\mathbf{H}')^* \cdot \mathbf{H} \right\} dxdz = 0. \tag{4.4}$$

This equality should hold for all trial fields $\mathbf{E}'$ and $\mathbf{H}'$.

Now the fields from equation (4.2) can be substituted for the $\mathbf{E}$ and $\mathbf{H}$ in equation (4.4). If for the trial fields the modal elements $\mathbf{E}_l$ and $\mathbf{H}_l$ are used the resulting integral should vanish for every l. Equation (4.4) then becomes

$$\sum_k K_{lk}a_k = 0 \text{ for all } l,$$

with

$$K_{lk} = \int \int \left\{ (\mathbf{H}_l)^* \cdot (\nabla \times \mathbf{E}_k) - (\mathbf{E}_l)^* \cdot (\nabla \times \mathbf{H}_k) - i\omega\varepsilon(\mathbf{E}_l)^* \cdot \mathbf{E}_k \right.$$
$$\left. -i\omega\mu_0(\mathbf{H}_l)^* \cdot \mathbf{H}_k \right\} dxdz. \qquad (4.5)$$

Since the input will only enter in the left side of waveguide 1, f_0^1 should be equal to 1 and b_N^1, f_0^2 and b_N^2 should be zero. Once these constants are substituted in a_k, the next step is to reorder a_k such that the given entries, $\mathbf{g}$ are at the top, followed by the unknowns $\mathbf{u}$ and build a matrix K which consists of all those K_{lk} in the order in which they appear in $\mathbf{a}$. This results in a system $K\mathbf{a}$ which looks like

$$\begin{bmatrix} K_{gg} & K_{gu} \\ K_{ug} & K_{uu} \end{bmatrix} \begin{bmatrix} \mathbf{g} \\ \mathbf{u} \end{bmatrix} = 0. \qquad (4.6)$$

Since the 4 elements of $\mathbf{g}$ are already given, this system has more equations than unknowns and is overdetermined.

To overcome this, the system will be solved in a least square sense, by rewriting (4.6) into $\begin{bmatrix} K_{gg} \\ K_{ug} \end{bmatrix} \mathbf{g} = - \begin{bmatrix} K_{gu} \\ K_{uu} \end{bmatrix} \mathbf{u}$ or $-K_g\mathbf{g} = K_u\mathbf{u}$. Now the unknown coefficients in $\mathbf{u}$ can be found by solving $-K_u^\dagger K_g\mathbf{g} = K_u^\dagger K_u\mathbf{u}$. Hence $\mathbf{u} = -(K_u^\dagger K_u)^{-1}K_u^\dagger K_g\mathbf{g}$. The symbol † indicates the adjoint.

The last step is to translate this solution back to the electric and magnetic fields. This is done by substituting the coefficients in $\mathbf{u}$ and $\mathbf{g}$ into equation (4.2). However, even without this back translation, the coefficients in $\mathbf{u}$ give important information. For instance, the coefficient which belongs to the element related to the drop port corresponds to the amplitude of the field at the left side of waveguide 2, its square corresponds to the relative amount of dropped power P_D. If this number is large the cavity must be in resonance. Further away from the resonance this number will be small. In the same way the P_F, P_T and P_R can be determined.

Chapter 5

Results

This chapter shows some results of the program that implements the formalism of the previous chapter. Section 5.1 gives some details on the implementation in Matlab. Section 5.2 shows what happens if two straight waveguides are coupled. In section 5.3 some results for the disc resonator are shown.

5.1   Some details of the Matlab program

The fields of the waveguides are calculated as mentioned in chapter 2. The propagation constant is determined for the wavelength parameter, or real frequency, as prescribed for the frequency domain formalism of chapter 4. This parameter also appears in equations (4.3), (4.4) and (4.5). For the cavity one or more resonances are determined using the program from section 2.3. The cavity resonances are determined only once, for angular wavenumbers m and radial orders such that the real parts of the frequency fall within the specified region of interest. If the program is run for a different wavelength, no new resonances are determined. Only whispering gallery modes which are well confined in the cavity are considered. Their complex frequency is only used for the fields of the cavity.

To calculate the integrals from equation (4.5) not only the electric and magnetic fields are needed, but also their derivatives. How these are determined for the cavity fields is described in appendix B. Once the electric and magnetic fields and their derivatives are known to the program, the integrals in equation (4.5) to fill the matrix from equation (4.6) can be determined. The integrals are evaluated numerically, using the Matlab function dblquad. This function needs the function which has to be integrated and the boundaries of the integration domain as parameters. This domain is determined as follows.

Due to the finite element discretization for the waveguides the integral in equation (4.5) has to be calculated only over the interval where the function α_j of

both of the nodes corresponding to the indices k and l is unequal to zero. This implies that the integral will automatically be set to zero if two nodes are not adjacent or equal. If these indices correspond to two adjacent nodes, the interval of integration will have a width of δz and if these indices correspond to the same node the integration will be over a width of $2\delta z$. This way the integration in the z-direction does not have to go from z_0 to z_N and calculations can be carried out much faster. Furthermore, this eliminates the possibility that the initial steps taken by the function dblquad are too large and the parts which are nonzero are missed, which otherwise might happen if δz is small.

Another thing which is used to improve the calculation time, is the assumption that the fields of a waveguide are zero if the distance to the waveguide is large. This can be done since the fields of the waveguides decay fast outside the waveguide. For the cavity the interior fields from the centre of the cavity to a suitable chosen radius are set to zero. This is allowed because for the whispering gallery modes under consideration the fields are only large in the area near the boundary of the cavity, and outside, as can be seen in figure 3.4. The calculation domain is limited to the region where the waveguides are near the circular cavity. This way the growing fields further away from the cavity can not disturb the results.

Since the calculation of the matrix K_{lk} is computationally heavy, this is not done for every new wavelength. Instead only two matrices corresponding to wavelengths suitably distributed over the wavelength region of interest are evaluated and the others are determined with simple linear inter- (extra-)polation. Suppose A_1 is the matrix corresponding to λ_1 and A_2 is the matrix corresponding to λ_2. Then the matrix corresponding to λ is estimated as

$$A(\lambda) = \frac{\lambda - \lambda_1}{\lambda_2 - \lambda_1} \left[A_2 - A_1 \right] + A_1.$$

The matrix depends on the wavelength through the basis mode profiles on the one hand and directly through equations (4.3a,b) on the other hand. Since the fields of the waveguide vary only slowly with the wavelength, the matrix itself will also change only slowly with the wavelength. This is why the estimate as explained here will be good. Peaks and dips in the transmission will still be found, since these are determined while solving the system (4.6). With this approximation the spectral response of the structure can be calculated much faster. Once an interesting feature has been found, the program can be run again without the interpolation procedure to obtain a more precise result, if necessary.

Although the formalism from chapter 4 and the limitations described above are not very difficult, implementation is a bit more complicated. Bookkeeping of the matrix elements needs some attention, to make sure that only the elements which should be nonzero are filled and each element is filled with the accompanying integral. Furthermore, one has make sure that all fields and their derivatives are given correctly. This seems straightforward, but these fields are quite complicated and mistakes might not always show.

5.2 Coupling of two straight waveguides

As a first test for the program two straight waveguides are placed close to each other. The horizontal computation window is discretized with $N = 500$ elements. Figure 5.1 shows the results. The light enters the lower waveguide from the left and after a certain distance all of it is coupled into the upper waveguide. Both waveguides have the same properties. Their refractive index is $n_g = 1.5$, the refractive index of the background is $n = 1$. The width of the waveguides is $0.4\mu m$ and they are placed $0.6\mu m$ out of the centre, hence the distance between them is $1.2\mu m$. The wavelength is $1.05\mu m$. According to [7] the distance required for this, the coupling length, is $1038\mu m$. This can also be seen from the figure.
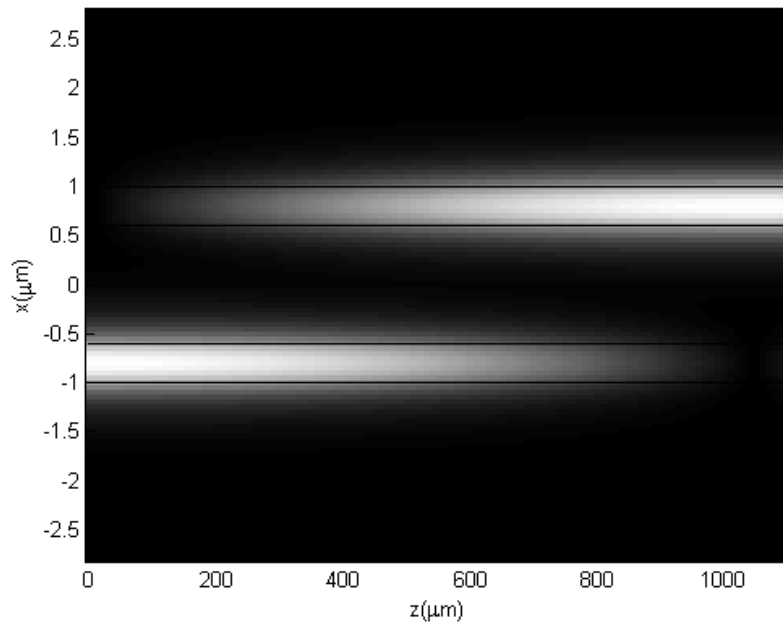
Figure 5.1: The absolute value of the electric field of two coupled straight waveguides.

If the same waveguides are placed $5.2\mu m$ out of the centre, thus the distance between them is $10.4\mu m$, there is no coupling and the field should (virtually) stay in the first waveguide. This is confirmed by the program, see figure 5.2.

The program is not suitable for a configuration where the waveguides are placed really close to each other, since it assumes that the superposition (4.1, without cavity modes) is a good approximation of the field of the composite structure. If the distance between two waveguides is very small, this assumption does not hold anymore. The results will show an interaction, however the coupling length will not be correct and thus the result will be useless.
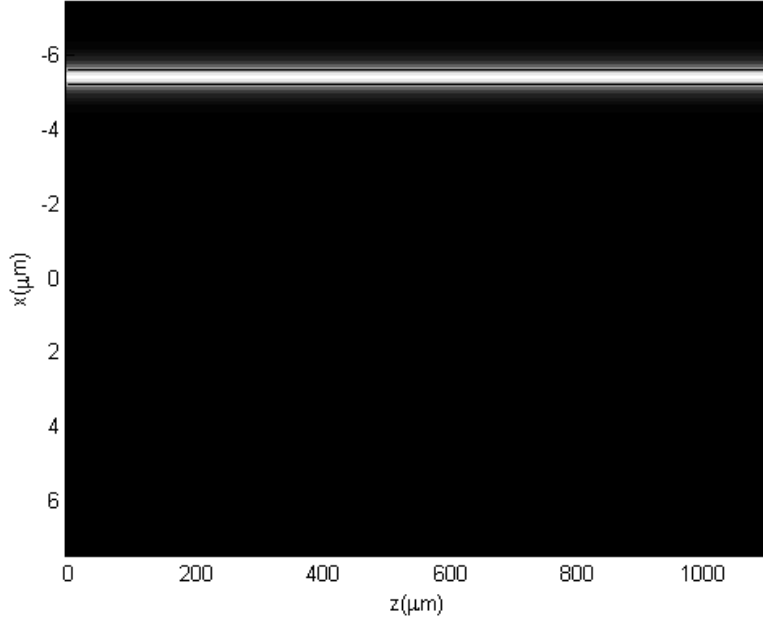
Figure 5.2: The absolute value of the electric field of two straight waveguides at a larger distance.

5.3 Coupling the disc cavity and the waveguides

After testing the program with only waveguides, the next step is to apply it to the kind of structures it was actually meant for, i.e. a circular disc cavity between two parallel straight waveguides. All results in this section have a computational window exactly equal to the size in the figures and a horizontal discretization in $N = 51$ pieces. At first only one whispering gallery mode, the one with $m = 40$, is taken into account and it can only propagate in one direction, also the fields in the waveguides can only propagate in one suitably chosen direction. The template (4.1) thus reads

$$\begin{bmatrix} \mathbf{E} \\ \mathbf{H} \end{bmatrix} (x, z) = f_1(z)\psi_1^+(x, z) + b_2(z)\psi_2^-(x, z) + \gamma_{40}\psi_3^{40}(x, z).$$

The result of a wavelength scan for that a simple model can be seen in figure 5.3.

Here both waveguides have thickness $0.4\mu m$, $g = 0.2\mu m$ and a refractive index of 1.5. The disc cavity has a radius of $5\mu m$ and also a refractive index of 1.5. The background refractive index equals 1. One can see that there is a dip in P_T and a peak in P_D. Figure 5.4 shows the power in the cavity, which is high near the resonance and low further away from it. This is exactly as was expected. In figure 5.5a, a snapshot of the electric field far away from the resonance is shown, figure 5.5b shows the same field, but now in resonance. Figure 5.6 shows how
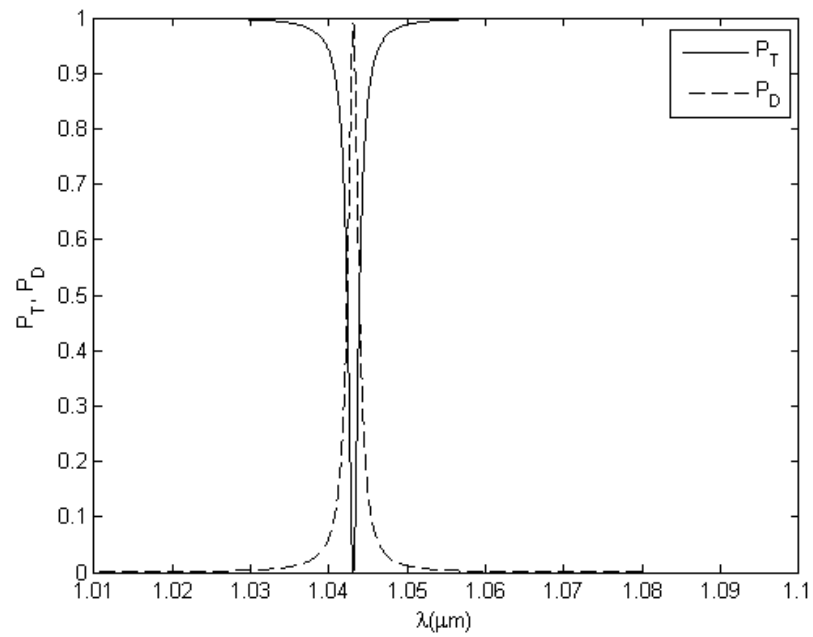
28

Figure 5.3: A scan of the normalized output power P_T on the right of the lower waveguide, waveguide 1, and P_D on the left of the upper waveguide, waveguide 2.

the absolute value and the real and imaginary part of the functions f_1 and b_2 behave at the resonance wavelength.
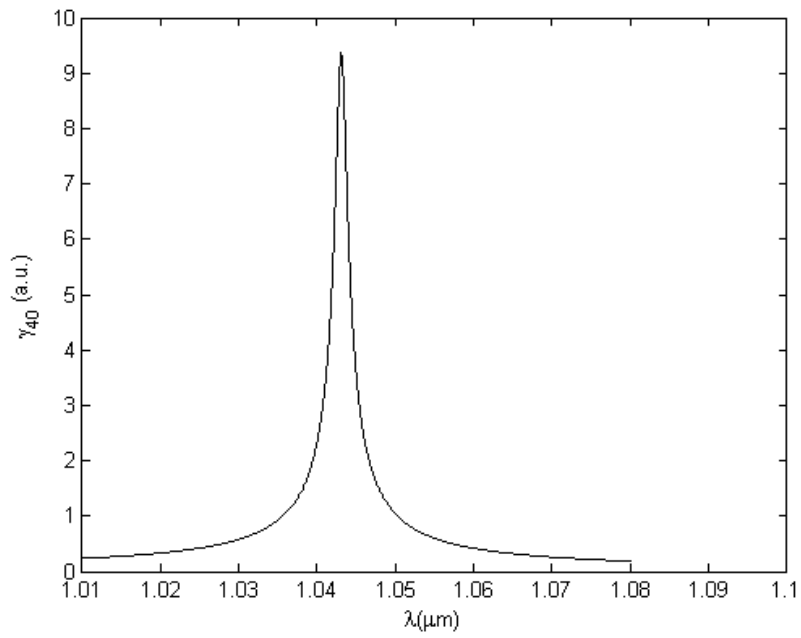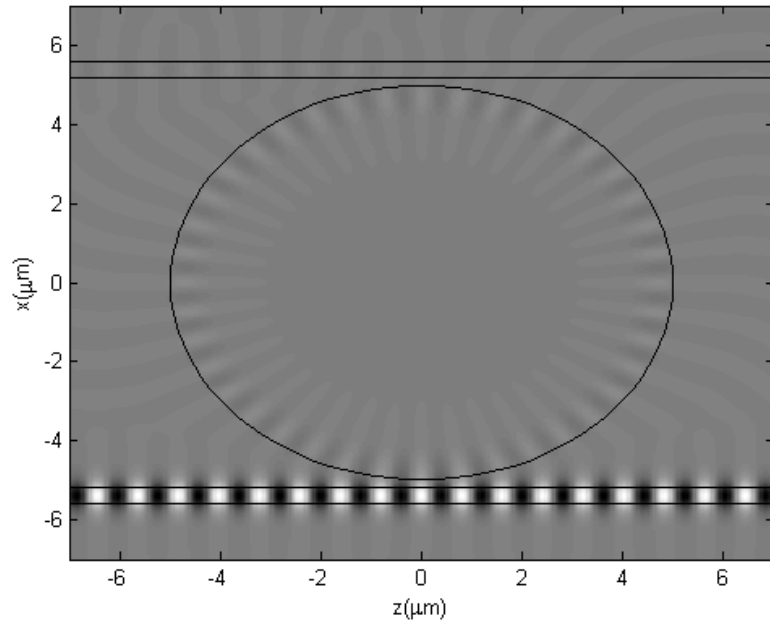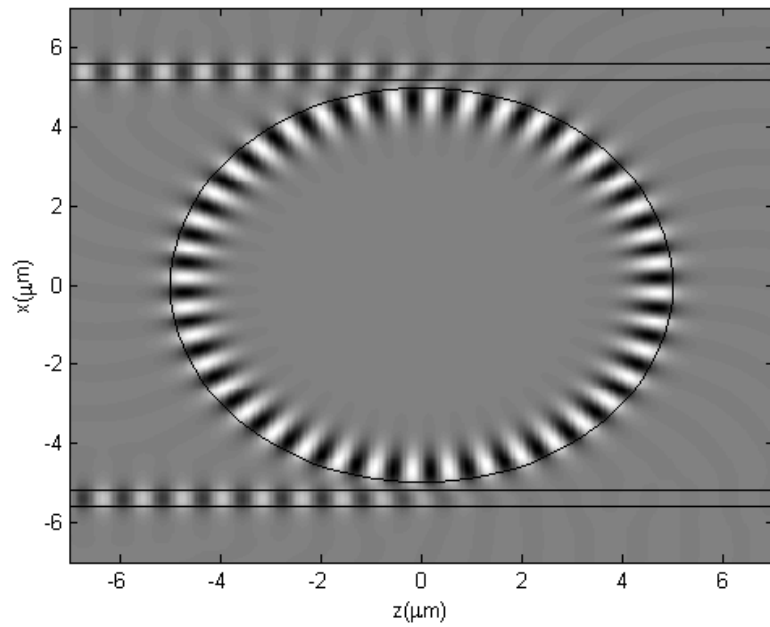
Figure 5.4: A scan of the coefficient γ_{40} of the whispering gallery mode with angular wavenumber $m = 40$.

(a)

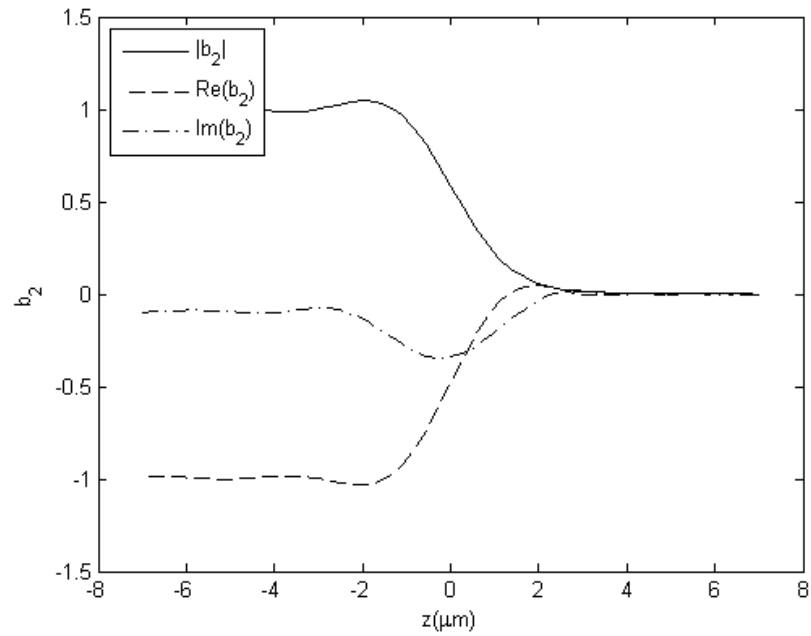
(b)

Figure 5.5: A snapshot of the electric field at $\lambda = 1.06\mu m$ (a), off resonance, and $\lambda = 1.043\mu m$ (b), in resonance.
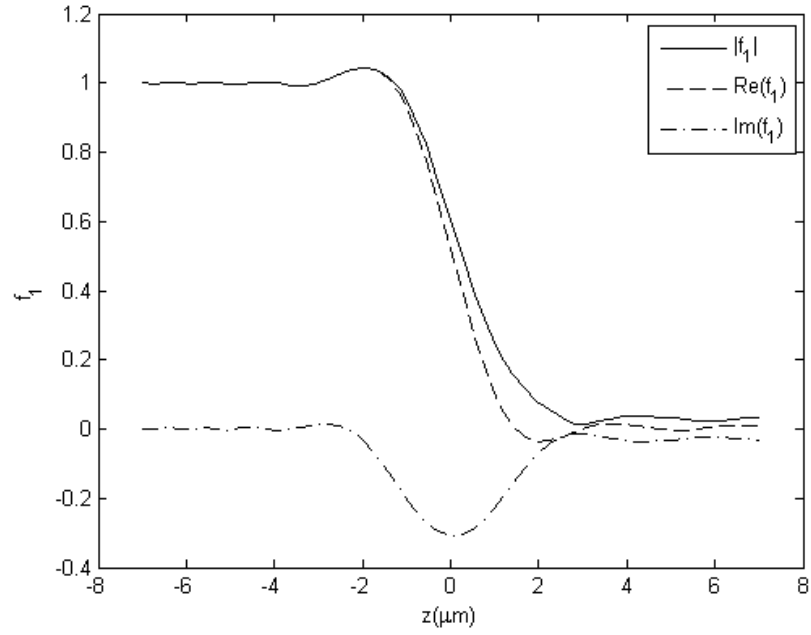
(a)

(b)

Figure 5.6: The absolute value and real and imaginary part of f_1, $\lambda = 1.043 \mu m$ (a) and b_2, $\lambda = 1.043 \mu m$ (b).

Since the previous results are good, also more realistic configurations will be tried. As a first step, other whispering gallery modes of the cavity could be added. One expects that further dips occur in the throughput and peaks in the drop curves, each corresponding to one of the cavity resonances. In figure 5.7 a scan with the same configuration as before is shown. In this case not only the whispering gallery mode of angular order $m = 40$ is taken into account, but also the ones with $m = 39$ and $m = 41$, all of the lowest radial order. The template (4.1) then reads

$$\begin{bmatrix} \mathbf{E} \\ \mathbf{H} \end{bmatrix} (x, z) = f_1(z)\psi_1^+(x, z) + b_2(z)\psi_2^-(x, z) + \sum_M \gamma_M \psi_3^M(x, z),$$

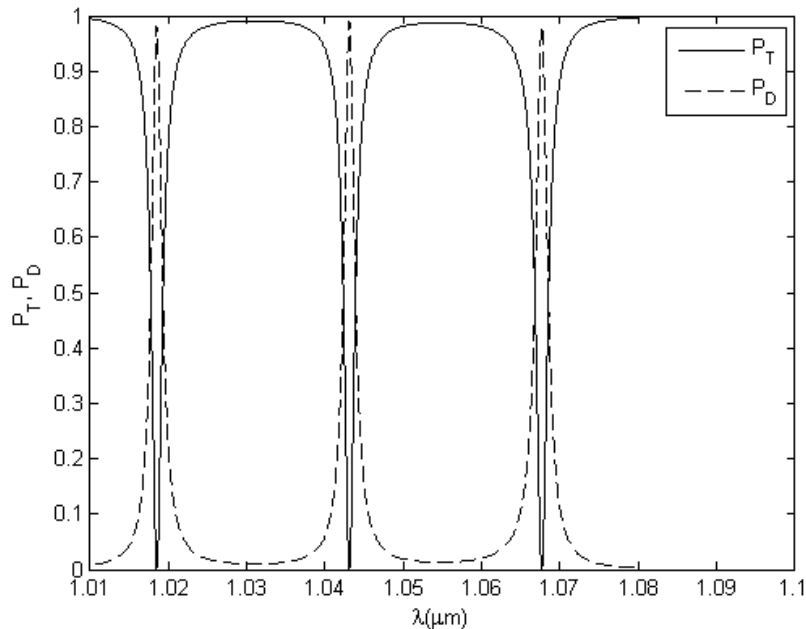where M includes only the whispering gallery modes mentioned before.

Figure 5.7: A wavelength scan including three whispering gallery modes.

In a physical situation not only modes of the lowest radial order will be present, but also fields of higher radial order if their resonance frequency falls within the spectral interval of interest. Since these higher modes are more lossy, it is likely that they will not couple as good as the principal modes. Still, they have influence on the behaviour of the cavity. This is why figure 5.8 shows a scan including the former whispering gallery modes and also three modes of first radial order that exist in the same wavelength region, with angular order $m = 34$, $m = 35$ and $m = 36$. Taking into account even higher order modes will again change the results, but probably not as much as here, since they will not contain a lot of power due to their losses. Figure 5.9 shows a snapshot of the field at $\lambda = 1.049$.
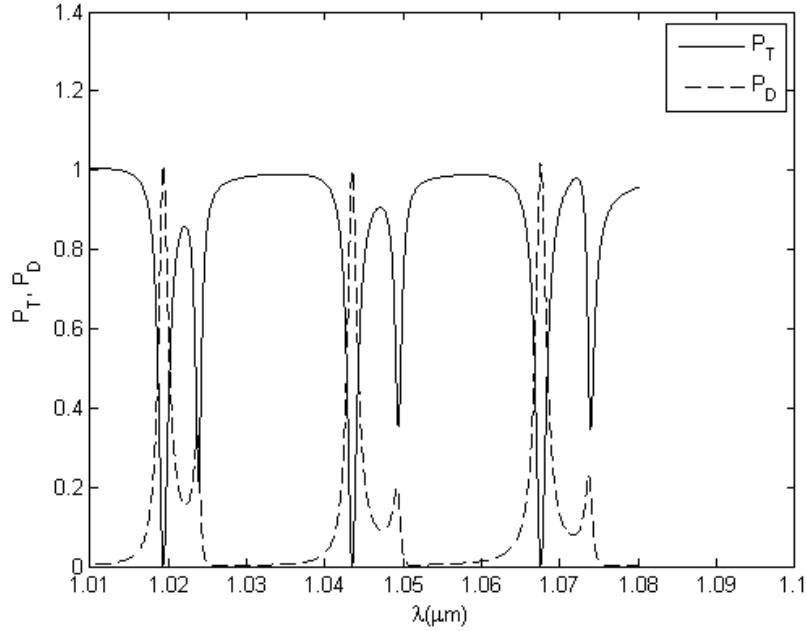
Figure 5.8: A wavelength scan for the microdisc including three modes of fundamental and three modes of first radial order.

The results compare well with the findings of [9] for the same structures. However, there is one striking difference. The power in the cavity fields levels on both sides of the cavity as can be seen in figure 5.5b. This is not the case in [9]. In a physical situation this will also not be the case, the fact that it occurs here has to do with the model. Since each whispering gallery mode has only one constant coefficient γ the model is unable to make a difference between both sides of the cavity.

To check whether the results do not depend too much on the size of the calculation window, the same scan is done with a larger calculation window. This time the z-axis extends from $-10\mu m$ to 10μ and the x-axis from $-10.4\mu m$ to $10.4\mu m$. Figure 5.10 shows the results, they look very similar to those from the previous scan.
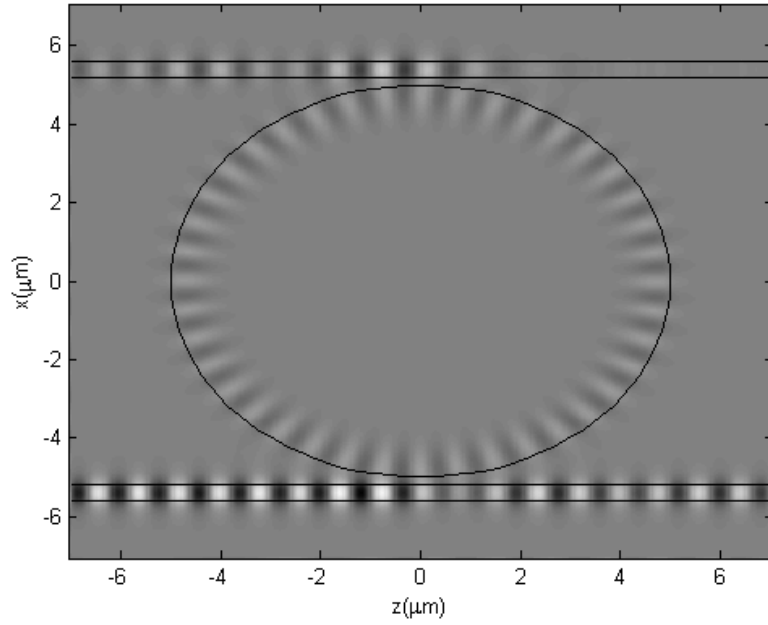
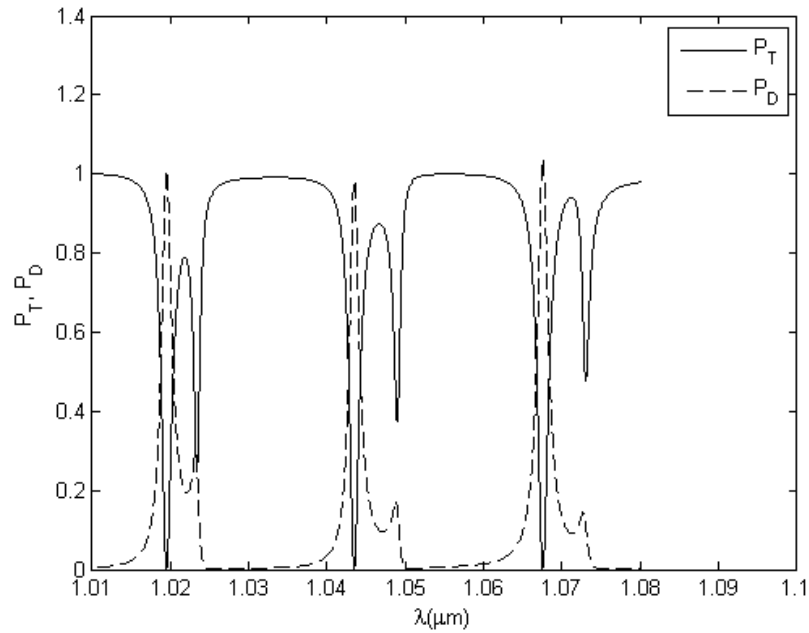Figure 5.9: A snapshot of the electric field of the microdisc with $\lambda = 1.049$.

Figure 5.10: A wavelength scan for the microdisc including three modes of fundamental and three modes of first radial order, with a larger calculation window than before.

5.4   Coupling the ring cavity and the waveguides

The last section showed some simulation results using a disc cavity, where this section shows some simulation results of a ring resonator. For this purpose the program is extended, such that it is able to handle ring microresonators. Since all fields are already known from chapter 2 this is not very complicated. All parameters are kept as before in the disc simulations, the only difference is that the disc is replaced by a ring with an inner radius $R_1 = 4.5$ and an outer radius $R_2 = 5$. The centre of the ring has refractive index $n = 1$, just like the exterior and the ring itself has a refractive index of $n = 1.5$, like the disc had in the previous section. This change makes that the resonances shift, so the resonance frequencies and angular wavenumbers m have to be determined again. Figure 5.11 shows a scan of the output in both waveguides, including only the whispering gallery mode with angular mode number $m = 39$. Figure 5.12 shows snapshots of the electric field in and off resonance.
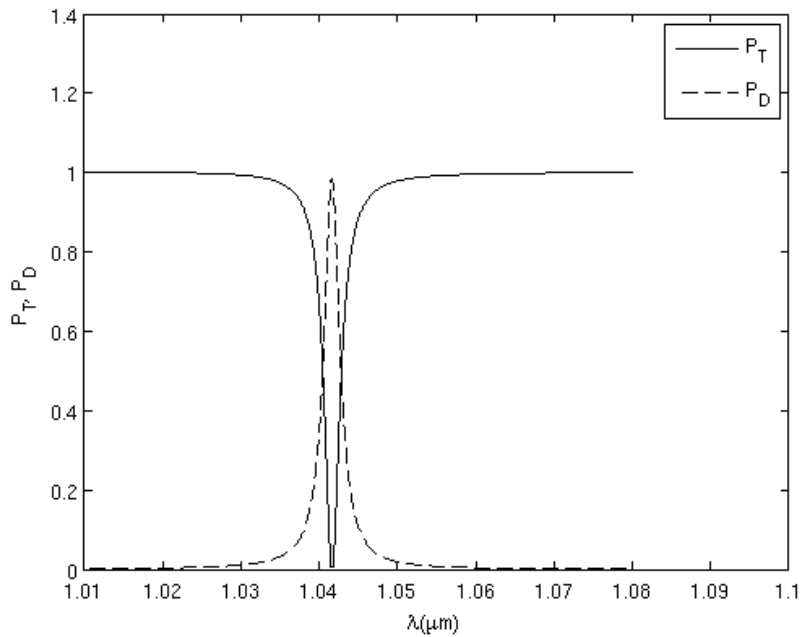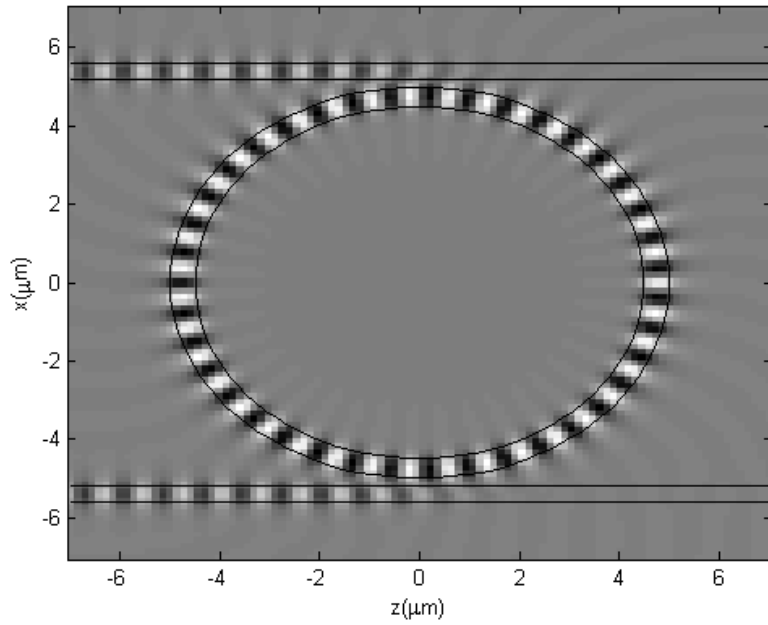

Figure 5.11: A wavelength scan of the ring resonator including only one mode.

As was done in the disc case, the program is now extended to be able to include several modes of angular order. Figure 5.13 shows the results of such a scan including the modes with angular wavenumbers $m = 38$, $m = 39$ and $m = 40$. Again the results are very similar to those in[9].
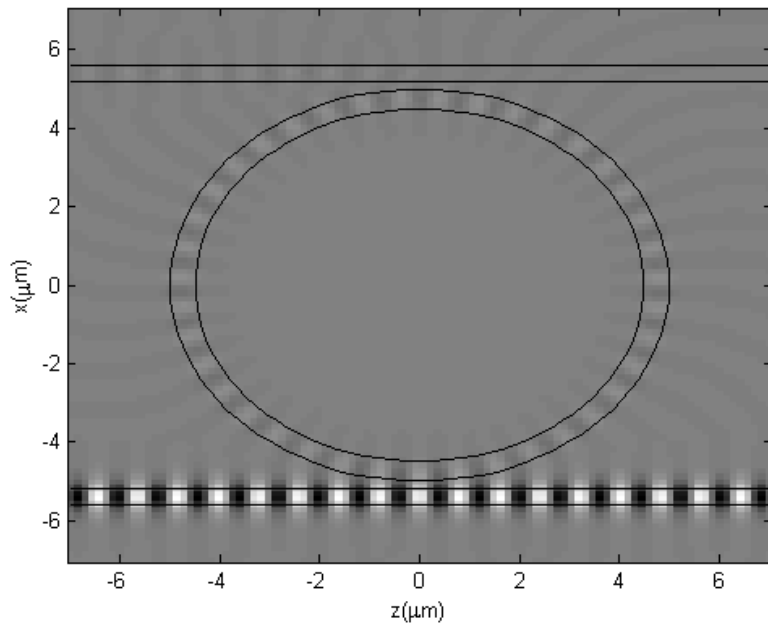
Figure 5.12: A snapshot of the electric field at $\lambda = 1.0416\mu m$ (a), in resonance, and $\lambda = 1.06\mu m$ (b), off resonance.

Figure 5.13: A wavelength scan of the ring resonator, including three modes of fundamental radial order.
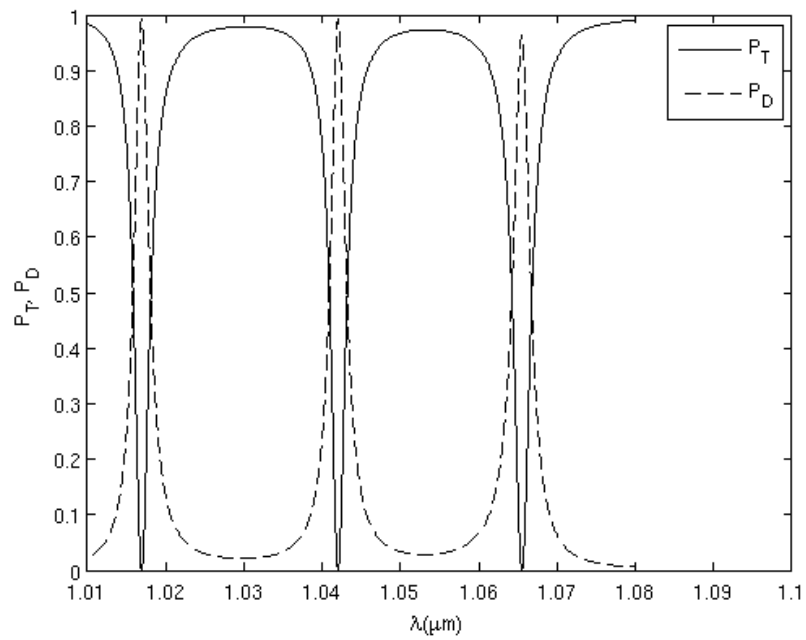
Chapter 6

Conclusions and further work

In this thesis a method to find the whispering gallery modes of a circular microresonator is explained. In principle this methods not only applies to a disc or ring, but also to circular structures with more layers. No complicated evaluations of Bessel functions of complex order have to be executed, as is required in a model based on the bent waveguide approach. Finding the complex frequency of the resonance is not very easy, due to the slow change in size of the determinant of the matrix as a function of the imaginary part of the frequency, as explained in chapter 2, but it can be done and has to be done only once for each structure and integer angular mode order. The results of the model explained here correspond well to the results found in literature, not only with results from other publications using whispering gallery modes, but also with results from the bent waveguide approach.

Using these whispering gallery modes a model for coupling a circular microresonator with two parallel straight waveguides was implemented. This model is based on coupled mode theory and makes use of a finite elements discretization of the modes supported by the straight waveguides. All of this was implemented in Matlab and tested with both a disc and a ring resonator, at first using only one whispering gallery mode. Since calculating the entire fields for several wavelengths is very time consuming, a scan is made by interpolating between wavelengths. The results from such a scan match very good with the results from [9], which were confirmed by FDTD calculations. Expanding the program such that it takes whispering gallery modes of higher radial order of the cavity into account also gives good results.

Since so far all results are very good, the method described in this thesis can be used as an alternative for time consuming FDTD calculations, at least for configurations for which the assumptions underlying the coupled mode template are valid.

6.1 Further work

Knowing that the model as described in this thesis works well, it could be interesting to do some more research on it. This can be done either to improve it or to expand it. One aspect which could use some improvement is finding the complex frequency of a whispering gallery mode. The way it is done now is accurate, but demands a very good estimate of the user. It would be preferable if this could be more automated, this would prevent human mistakes like typing errors and increase the speed, since the user now has to search for a good initial guess by hand.

The program might also be enhanced by allowing the light to propagate in both directions. The model is able to handle such situations, however all results given in this thesis assume light only propagates in one direction. It is likely that even if it is allowed to propagate in both directions, by far the largest part will still travel in the direction which is forced upon it now.

Another improvement would be expanding the program such that it can not only handle this simple structure with two straight waveguides and one cavity, but also more complicated structures. This could for instance include several cavities, with either the same or different properties. In principle all building blocks for such a structure are available, but combining them will give some difficulties. The complication is that at present the resonator is supposed to be originated at the origin. Of course it is possible to move it, but that will make the translation from Cartesian to the correct cylindrical coordinates slightly more difficult. Besides that, depending on the placement of the cavities, in some or all cavities modes with both positive and negative angular wavenumber m should be taken into account to get the desired results. This is not very complicated since the program in principle already allows it, but calculation times will grow.

One could also think about extending the model to the TM polarization. In that case the fields as calculated in chapter 2 can not be used, but they have to be replaced by fields that satisfy the other set of equations, those for E_x, E_z and H_y. Once the fields of the waveguides and cavity are determined in this case, the coupling can be estimated in the same way as is done in the TE case.

Thus far the whole model is 2D, but it should be possible to expand it into 3D. However, in 3D the Maxwell equations do not split up to two polarizations, hence it is impossible to calculate the mode profiles analytically. They can be replaced by numerically calculated mode profiles in 3D. Obviously the 3D calculations will be heavier than the 2D calculations, however, they will probably be much easier than rigorous numerical calculations.

Bibliography

[1] M. Abramowitz and I.A. Stegun. *Handbook of mathematical functions with formulas, graphs, and mathematical tables.* Dover publications, 1964.

[2] D.K. Cheng. *Field and wave electromagnetics.* Addison-Wesley Reading, MA, 1983.

[3] I.D. Chremmos and N.K. Uzunoglu. Analysis of coupling between two slab waveguides in the presence of ring resonators. *Journal of the Optical Society of America A*, 21(2):267–279, 2004.

[4] J. Čtyrokỳ, L. Prkna, and M. Hubalek. Guided-wave optical microresonators: Calculation of eigenmodes. In *AIP Conference Proceedings*, volume 709, page 72, 2004.

[5] WA Gambling. The rise and rise of optical fibers. *IEEE journal of selected topics in quantum electronics*, 6(6):1084–1093, 2000.

[6] David J. Griffiths. *Introduction to electrodynamics.* Prentice-Hall International, third edition edition, 1999.

[7] M. Hammer. 1-D multilayer slab waveguide mode solver. http://wwwhome.math.utwente.nl/ hammerm/oms.html.

[8] M. Hammer. Hybrid analytical/numerical coupled-mode modeling of guided-wave devices. *Journal of Lightwave Technology*, 25(9):2287–2298, 2007.

[9] K.R. Hiremath. *Coupled mode theory based modeling and analysis of circular optical microresonators.* PhD thesis, Twente University, 2005.

[10] KR Hiremath, M. Hammer, R. Stoffer, L. Prkna, and J. Čtyrokỳ. Analytic approach to dielectric optical bent slab waveguides. *Optical and Quantum Electronics*, 37(1):37–61, 2005.

[11] KR Hiremath, R. Stoffer, and M. Hammer. Modeling of circular integrated optical microresonators by 2-D frequency domain coupled mode theory. *Optics communications*, 257(2):277–297, 2006.

[12] C. Koos, M. Fujii, C.G. Poulton, R. Steingrueber, J. Leuthold, and W. Freude. FDTD modelling of dispersive nonlinear ring resonators: accuracy studies and experiments. *IEEE J. Quantum Electron*, 42:1215–1223, 2006.

[13] BE Little, ST Chu, W. Pan, D. Ripin, T. Kaneko, Y. Kokubun, and E. Ippen. Vertically coupled glass microring resonator channel dropping filters. *IEEE Photonics Technology Letters*, 11(2):215–217, 1999.

[14] A. Morand, K. Phan-Huy, Y. Desieres, and P. Benech. Analytical study of the microdisk's resonant modes coupling with a waveguide based on the perturbation theory. *Journal of Lightwave Technology*, 22(3):827, 2004.

[15] K. Okamoto. *Fundamentals of optical waveguides*. Academic press, 2000.

[16] L. Prkna, J. Čtyrokỳ, and M. Hubálek. Ring microresonator as a photonic structure with complex eigenfrequency. *Optical and Quantum Electronics*, 36(1):259–269, 2004.

[17] R. Ramaswami. Optical fiber communication: From transmission to networking. *IEEE Communications Magazine*, 40(5):138–147, 2002.

[18] DR Rowland and JD Love. Evanescent wave coupling of whispering gallery modes of a dielectric cylinder. *IEEE Proceedings J. Optoelectronics*, 140(3):177–88, 1993.

[19] A. Sakai and T. Baba. FDTD simulation of photonic devices and circuits based on circular and fan-shaped microdisks. *Journal of lightwave technology*, 17(8):1493, 1999.

[20] H. Sobol. Microwave Communications–An Historical Perspective. *IEEE Transactions on microwave theory and Techniques*, 32(9):1170–1181, 1984.

[21] Č. vysoké učení technické v Praze. Nové směry v integrované optice Novel Trends in Integrated Optics.

Appendix A

The Q-factor

This appendix explains in some detail how the results from the complex frequency model, as used in this thesis, can be compared to the results from the bent waveguide approach, as used in [9] for instance. The key ingredient is the so called Q-factor, short for quality factor. The Q-factor is a dimensionless property which describes, as the name says, the quality of the cavity. A high Q-factor implies low losses. This is a property of the structure, so it should be independent of the approach.

The complex frequency approach uses, as the name indicates, a complex frequency $\omega = \omega' + i\omega''$, where the bent waveguide approach deals with a real frequency ω_r. With the latter approach the propagation constant $\gamma = \beta + i\alpha$ is a complex number. The angular mode number is γR and the integer angular mode number is given by βR. In the complex frequency approach this is denoted with m.

For the complex frequency approach the Q-factor is defined by $Q \approx -\frac{\omega'}{2\omega''}$ and for the bent waveguide approach it is $Q \approx \frac{\beta}{2\alpha}$ [4, 16].

In a resonant configuration with approximately equal real frequency, $\omega' \approx \omega_r$, and integer angular mode number, $m \approx \beta R$, and low losses, such that $\alpha\omega'' \approx 0$, they should produce the same Q-factor. Now

$$-\frac{\omega'}{2\omega''} = \frac{\beta R}{2\alpha R}$$
$$\Leftrightarrow -\frac{\omega'}{\omega''} = \frac{\beta R}{\alpha R}$$
$$\Leftrightarrow -\alpha R\omega' = \beta R\omega''$$
$$\Leftrightarrow i\beta R\omega'' + i\alpha R\omega' \approx 0$$
$$\Leftrightarrow \beta R\omega' + i\beta R\omega'' + i\alpha R\omega' - \alpha R\omega'' \approx \beta R\omega' \approx m\omega_r$$
$$\Leftrightarrow (\omega' + i\omega'')(\beta + i\alpha)R \approx m\omega_r$$
$$\Leftrightarrow \frac{m}{\omega} \approx \frac{(\beta + i\alpha)R}{\omega_r} = \frac{\gamma R}{\omega_r}$$

Thus the an equal Q-factor implies that $\frac{m}{\omega}$ and, in the bent waveguide approach, $\frac{\gamma R}{\omega_r}$ should be approximately equal. This justifies the comparison of $\frac{mc}{R\omega}$ as used in chapter 2. Written in the quantities of the bent waveguide approach this is exactly $\frac{\gamma}{k_0}$, with $k_0 = \frac{\omega}{c}$.

Appendix B

Derivatives of the cavity fields

On several places in this report derivatives of the cavity fields are used. This appendix gives some insight in how they are calculated and implemented. The first section gives the r-derivative of the electric field of the cavity, which is used in chapter 2. The second and third section explain how the x- and z-component of the magnetic fields are calculated, which are used in chapter 4.

B.1   Derivative with respect to r

To calculate the resonance frequency in section 2.3 the electric field has to be differentiated with respect to r, in order to obtain continuity of the magnetic field at the interfaces. For this, derivatives of Bessel functions are required. These derivatives are given by

$$\frac{d}{dx}y_p(\alpha x) = \frac{\alpha}{2}\left[y_{p-1}(\alpha x) - y_{p+1}(\alpha x)\right],$$

where y can be either the Bessel function of the first or second kind or the Hankel function of the first or second kind [1].

From this, all necessary derivatives can easily be calculated. As an example, the r-derivative of the electric field in the centre region is given here. Recall that in this region

$$E_y(r) = a_1 J_m(\frac{\omega}{c}n_1 r).$$

Thus, in this case the r-derivative will be given by

$$\frac{d}{dr}E_y(r) = a_1 \frac{\omega n_1}{2c}\left[J_{m-1}(\frac{\omega}{c}n_1 r) - J_{m+1}(\frac{\omega}{c}n_1 r)\right].$$

In this case the factor $e^{im\varphi}$ can be omitted, since this does not influence the r-derivative.

B.2 Derivative with respect to x

Finding the derivative with respect to x is a bit more complicated, since x is hidden in r and φ through the relations

$$
\begin{aligned}
r &= \sqrt{x^2 + z^2}, \\
\tan(\varphi) &= \frac{x}{z}.
\end{aligned}
$$

Now the factor $e^{im\varphi}$ has to be taken into account, since it contains φ which hides x. As an example the x-derivative of the same field as in the example in section B.1 is given here. The original field was given as:

$$
\begin{aligned}
E_y(r, \varphi) &= a_1 J_m(\frac{\omega}{c} n_1 r) e^{im\varphi} \\
\Rightarrow E_y(x, z) &= a_1 J_m(\frac{\omega}{c} n_1 \sqrt{x^2 + z^2}) e^{im\tan^{-1}\left(\frac{x}{z}\right)}.
\end{aligned}
$$

Differentiating with respect to x is not very difficult and gives

$$
\frac{d}{dx} E_y(x, z) = a_1 \left[\frac{\omega n_1 x \left(J_{m-1}(\frac{\omega}{c} n_1 \sqrt{x^2 + z^2}) - J_{m+1}(\frac{\omega}{c} n_1 \sqrt{x^2 + z^2}) \right)}{c\sqrt{x^2 + z^2}} \right. \\
\left. + \frac{im J_m(\frac{\omega}{c} n_1 \sqrt{x^2 + z^2})}{z(1 + \frac{x^2}{z^2})} \right] e^{im\tan^{-1}\left(\frac{x}{z}\right)}.
$$

However, due to the division through z a singularity arises wherever z is equal to zero. To overcome this, the former equation can be rewritten to

$$
\frac{d}{dx} E_y(x, z) = a_1 \left[\frac{\omega n_1 x \left(J_{m-1}(\frac{\omega}{c} n_1 \sqrt{x^2 + z^2}) - J_{m+1}(\frac{\omega}{c} n_1 \sqrt{x^2 + z^2}) \right)}{c\sqrt{x^2 + z^2}} \right. \\
\left. + \frac{imz J_m(\frac{\omega}{c} n_1 \sqrt{x^2 + z^2})}{z^2 + x^2} \right] e^{im\tan^{-1}\left(\frac{x}{z}\right)}.
$$

Now only the origin has a singularity, this is not a problem, since the electric field is approximately zero in and close to the origin, so its derivative will also be zero. In the program from chapter 5 the centre of the cavity is disregarded upto a suitably chosen radius. This decreases calculation time, since the integral does not have to be calculated in a region where it is known that the function is almost zero.

B.3 Derivative with respect to z

Differentiating with respect to z is not very different from differentiating with respect to x. In the example of above the z-derivative will be

$$\frac{d}{dz}E_y(x,z) = a_1 \left[\frac{\omega n_1 z \left(J_{m-1}(\frac{\omega}{c}n_1\sqrt{x^2+z^2}) - J_{m+1}(\frac{\omega}{c}n_1\sqrt{x^2+z^2}) \right)}{c\sqrt{x^2+z^2}} \right.$$
$$\left. - \frac{imx J_m(\frac{\omega}{c}n_1\sqrt{x^2+z^2})}{z^2(1+\frac{x^2}{z^2})} \right] e^{im\tan^{-1}\left(\frac{x}{z}\right)}.$$

Again the problem with the division through z arises, so the equation is rewritten to

$$\frac{d}{dz}E_y(x,z) = a_1 \left[\frac{\omega n_1 z \left(J_{m-1}(\frac{\omega}{c}n_1\sqrt{x^2+z^2}) - J_{m+1}(\frac{\omega}{c}n_1\sqrt{x^2+z^2}) \right)}{c\sqrt{x^2+z^2}} \right.$$
$$\left. - \frac{imx J_m(\frac{\omega}{c}n_1\sqrt{x^2+z^2})}{z^2+x^2} \right] e^{im\tan^{-1}\left(\frac{x}{z}\right)}.$$